RADC-TR-88-109
Final Technical Repor
June 1988

AD-A198 783

SELF-COHERING AIRBORNE DISTRIBUTED ARRAY

INTERSPEC Incorporated

Dr. E. Hesham Attia

APPROVED FOR PUBLIC RELEASE; DISTRIBUTION UNLIMITED.

ROME AIR DEVELOPMENT CENTER
Air Force Systems Command
Griffiss AFB, NY 13441-5700

UNCLASSIFIED
SECURITY CLASSIFICATION OF THIS PAGE

REPORT DOCUMENTATION PAGE

Form Approved OMB No. 0704-0188

1a. REPORT SECURITY CLASSIFICATION UNCLASSIFIED	1b. RESTRICTIVE MARKINGS N/A
2a. SECURITY CLASSIFICATION AUTHORITY N/A	3. DISTRIBUTION/AVAILABILITY OF REPORT Approved for public release; distribution unlimited
2b. DECLASSIFICATION/DOWNGRADING SCHEDULE N/A	
4. PERFORMING ORGANIZATION REPORT NUMBER(S) R-174	5. MONITORING ORGANIZATION REPORT NUMBER(S) RADC-TR-88-109
6a. NAME OF PERFORMING ORGANIZATION INTERSPEC Incorporated 6b. OFFICE SYMBOL (If applicable)	7a. NAME OF MONITORING ORGANIZATION Rome Air Development Center (EEAS)
6c. ADDRESS (City, State, and ZIP Code) 1100 East Hector Street Conshohocken PA 19428	7b. ADDRESS (City, State, and ZIP Code) Hanscom AFB MA 01731-5000
8a. NAME OF FUNDING/SPONSORING ORGANIZATION Rome Air Development Center 8b. OFFICE SYMBOL (If applicable) EEAS	9. PROCUREMENT INSTRUMENT IDENTIFICATION NUMBER F19628-84-C-0080
8c. ADDRESS (City, State, and ZIP Code) Hanscom AFB MA 01731-5000	10. SOURCE OF FUNDING NUMBERS PROGRAM ELEMENT NO. 61102F; PROJECT NO. 2305; TASK NO. J3; WORK UNIT ACCESSION NO. 46

11. TITLE (Include Security Classification)
SELF-COHERING AIRBORNE DISTRIBUTED ARRAY

12. PERSONAL AUTHOR(S)
Dr. E. Hesham Attia

13a. TYPE OF REPORT	13b. TIME COVERED	14. DATE OF REPORT (Year, Month, Day)	15. PAGE COUNT
Final	FROM Jan 84 TO Oct 85	June 1988	54

16. SUPPLEMENTARY NOTATION
N/A

17. COSATI CODES			18. SUBJECT TERMS (Continue on reverse if necessary and identify by block number)		
FIELD	GROUP	SUB-GROUP	Radar	Conformal Arrays	Radar Clutter
09	01		Self-Cohering	Adaptive Beamforming	
17	07, 11		Phased Arrays	Airborne Radar	

19. ABSTRACT (Continue on reverse if necessary and identify by block number)

Several algorithms for self cohering an airborne distributed array on radar clutter have been tested and their performances have been statistically evaluated. Also, several new algorithms have been developed. The new algorithms offer, in general, improved performance and wider applicability.

Airborne clutter data was obtained from two sources: the Naval Research Laboratory (NRL) and the Environmental Research Institute of Michigan (ERIM). Specific runs of the 8-element NRL airborne array were identified and obtained. These covered land as well as sea clutter, with different radar look angles, and different pulse repitition rates. Several runs of ERIM SAR data were also obtained. The SAR data was adapted to permit testing of the "Minimum Variance" and "Robust" algorithms.

The performance of the Minimum Variance algorithm was tested and statistically evaluated using the NRL and ERIM clutter data. The algorithm was successful against land clutter (over)

20. DISTRIBUTION/AVAILABILITY OF ABSTRACT	21. ABSTRACT SECURITY CLASSIFICATION
☐ UNCLASSIFIED/UNLIMITED ☒ SAME AS RPT. ☐ DTIC USERS	UNCLASSIFIED
22a. NAME OF RESPONSIBLE INDIVIDUAL Robert A. Shore	22b. TELEPHONE (Include Area Code) (617) 377-2058 22c. OFFICE SYMBOL RADC (EEAS)

DD Form 1473, JUN 86 *Previous editions are obsolete.* SECURITY CLASSIFICATION OF THIS PAGE

UNCLASSIFIED

UNCLASSIFIED

Block 19. Abstract (Cont'd)

where it was used successfully for finding targets of opportunity that allowed retrodirective beamforming. The algorithm was unreliable (as expected) against sea clutter.

Doppler Beamsharpening techniques were also tested against the NRL land clutter data. Doppler Beamsharpening proved to be highly effective in increasing the chance of finding targets of opportunity that allow high quality retrodirective beamforming.

Several new algorithms were developed during this study. We developed and tested the Robust Minimum Variance Algorithm to provide reliable beamforming on a collection of inferior beamformers (targets of opportunity). We also developed and tested the Spatial Correlation Algorithm which is applicable to sea as well as to land clutter. It allows also for local processing within the aperture, in contrast to transmitting information for each module to a central processor. This makes it attractive for a cost effective large aperture space based radar. Finally, we developed a technique of Subarray Processing for applying the above new algorithms on very large airborne or spaceborne radar systems.

TABLE OF CONTENTS

Page

1. SUMMARY OF RESULTS.....1

2. INTRODUCTION.....2

3. CLASSIFICATION OF SELF-COHERING ALGORITHMS.....3

4. STUDY RESULTS.....4

4.1 Task 1: Minimum Variance Algorithm.....4

4.1.1 Procedure.....4
4.1.2 Beamformer Quality.....6
4.1.3 Statistics of $\hat{\sigma}_{\delta\phi}$.....8
4.1.4 Application to NRL Land Clutter Data.....9
4.1.5 Application to ERIM SAR Land Clutter Data.....10
4.1.6 Application to Sea Clutter.....12

4.2 Task 2: Clutter Data Sources.....14

4.2.1 NRL 8-Element Array Data.....14
4.2.2 ERIM SAR Data.....15

4.3 Task 3: Doppler Algorithms.....16

4.3.1 Doppler Beam Sharpening.....16
4.3.2 Minimum Clutter Bandwidth.....19

4.4 Task 4: New Algorithm Development.....20

4.4.1 Robust Minimum Variance Algorithm.....20
4.4.2 Spatial Correlation Algorithm.....27
4.4.3 Subarray Processing.....33

5. CONCLUSIONS.....35

6. RECOMMENDATIONS FOR FUTURE WORK.....36

6.1 Spatial Correlation Processing Studies.....36

6.2 Robust Minimum Variance Studies.....36

7. REFERENCES.....38

APPENDIX A: THE RADIO CAMERA ALGORITHM.....A.1

A.1 Adaptive Beamforming.....A.1
A.2 Scanning.....A.3
A.3 Element Position Tolerance.....A.4

APPENDIX B: STATISTICS OF GEOMETRICAL PHASE ERRORS.....B.1

1. SUMMARY OF RESULTS

Several algorithms for self cohering an airborne distributed array on radar clutter have been tested and their performances have been statistically evaluated. Also, several new algorithms have been developed throughout the course of the study. The new algorithms offer, in general, improved performance and wider applicability.

We obtained airborne clutter data from two sources (Task 2): the Naval Research Laboratory (NRL) and the Environmental Research Insitute of Michigan (ERIM). We identified and obtained specific runs of the 8-Element NRL airborne array. These covered land as well as sea clutter, different radar look angles, and different pulse repetition rates. We also obtained several runs of ERIM SAR data. We adapted the use of SAR data to permit testing of the "Minimum Variance" and "Robust" algorithms.

We tested and statistically evaluated the performance of the Minimum Variance algorithm (Task 1) using the NRL and ERIM clutter data. The algorithm was successful against land clutter where it was used successfully for finding targets of opportunity that allowed retrodirective beamforming. The algorithm was unreliable (as expected) against sea clutter.

We also tested Doppler Beamsharpening techniques (Task 3) against the NRL land clutter data. Doppler Beamsharpening proved to be highly effective in increasing the chance of finding targets of opportunity that allow high quality retrodirective beamforming.

We developed several new algorithms (Task 4) during this study. We developed and tested the Robust Minimum Variance Algorithm to provide reliable beamforming on a collection of inferior beamformers (targets of opportunity). We also developed and tested the Spatial Correlation Algorithm which is applicable to sea as well as to land clutter. It allows also for local processing within the aperture, in contrast to transmitting information from each module to a centralized rigid processor, which makes it attractive for a cost effective large aperture space based radar. Finally, we developed a technique of Subarray Processing for applying the above new algorithms on very large airborne or spaceborne radar systems.

2. INTRODUCTION

The objective of this effort is to investigate techniques that can be used to mount airborne phased array radar antennas on arbitrary portions of the airframe. Current airborne phased arrays cannot be so mounted because the nonrigidity of the surface would severely degrade the phase coherence necessary for effective phased array performance. The ability to distribute the elements of a phased array over the entire aircraft will greatly enhance the ability of airborne radar systems to function in sophisticated battle environments.

The performance of an airborne radar antenna array is limited in several highly important respects by the fact that the array can be mounted only on certain sections of the aircraft. This localization of the antenna results in incomplete surveillance coverage and restricted freedom of communication with all desired stations. The restricted antenna aperture also limits the usable detection range of the radar and the angular resolution of the system, and makes the radar more susceptible to mainbeam jamming. These limitations could be greatly reduced if arrays could be installed in any arbitrary portion of the airframe. Air Force supported work in the past five years has shown that there is promise in designing radar antenna arrays to make use of arbitrary portions of the airframe. The key idea behind the use of such arrays is to make use of a portion of the scattered return of the radar signal to self-cohere the phases of the array elements and so compensate for the distortion in phase caused by the nonrigidity of the skin and airframe that would otherwise severly degrade the antenna performance. Not all scattered radar returns are useful for this purpose, however, and it is important to investigate the statistics of realistic radar clutter returns to see if systems can be designed to utilize these returns for self-synchronizing. The objective of this work is to identify existing sources of useful data and, using these data, to test and compare various algorithms for synchronizing the array.

3. CLASSIFICATIONS OF SELF-COHERING ALGORITHMS

Table 3.1 gives a classification of the self-cohering algorithms under consideration (including the newly developed algorithms). The algorithms are classified both according to the type of processing and according to the environment.

Regarding the type of processing, we classify the algorithms according to whether or not Doppler processing is used. It is worthwhile, however, to note that Doppler and non-Doppler techniques can be combined in some cases to come up with superior algorithms. For example, and as will become clear later on, the Doppler Beamsharpening techniques can be significantly enhanced by coupling the Doppler time-domain processing with the Robust space (or range bin)-domain processing.

With respect to the environment, we distinguish between the situation where the reradiating scatterers are rigid, which is found only in land clutter, and the situation where the scatterers undergo appreciable movement (in units of wavelength) due to wind as found in vegetation and sea clutter.

TABLE 3.1 CLASSIFICATION OF SELF-COHERING ALGORITHMS

	Non-Doppler	Doppler
Land Clutter	• Minimum Variance • Robust Minimum Variance • Spatial Correlation	• Doppler Beam Sharpening • Hybrid
Wind Driven Land Clutter and Sea Clutter	• Spatial Correlation	• Minimum Clutter Bandwidth

4. STUDY RESULTS

In this section we give a detailed report of study results. The section is organized according to contract tasks. For the sake of continuity, lengthy details and long mathematical deviations are defered to appendices.

4.1 TASK 1: MINIMUM VARIANCE ALGORITHM

Figure 4.1 shows a high angular resolution bistatic radar system that consists of a pulsed transmitter and a large distributed thinned array of receivers. In principal, the system can be ground based or airborne. For a ground based system the size of the receiving array can be increased to the extent that angular resolving powers comparable to common optical instruments such as cameras and small telescopes can be achieved. This system has been introduced in the literature [1], [2] as a "radio camera" capable of "taking pictures"of microwave scattering objects. For an airborne application, the size of the receiving array will be limited only by the size of the airframe. Yet, and as mentioned earlier, an airborne phased array radar flush mounted on arbitrary portions of the airframe offers many advantages over existing phased array systems which tend to be much smaller in size in order to maintain a rigid structure.

Such a large airborne antenna system has to be self-adaptive, i.e., the beam must be formed by a self-cohering process. Otherwise, the nonrigidity of the surface would severly degrade the phase coherence necessary for effective phased array performance. The basic idea is to find a suitable reference source, use adaptive retrodirective beamforming techniques to focus the large distorted array on it, and then move the narrow focused beam in range and angle to a target area and scan the beam across the target.

It is shown in [1], [2] that a suitable reference should approximate a point source, strong enough to overcome clutter (about 6 dB higher). That is, it should have the right combination of small physical size (in terms of wavelength) and strong echo. In a ground based system, the phase synchronizing source can be a corner reflector, a beacon, or a target of opportunity (TOO). In an airborne system, the basic algorithm should rely only on finding suitable TOO's. The minimum variance algorithm was developed to do exactly that [2].

4.1.1 PROCEDURE

Figure 4.1 describes the procedure explicitly. A ground-to-ground imaging situation is portrayed. On the left are a radar transmitter and receiver. The target region to be imaged is on the right. A transmitted pulse illuminates the target area and a passive phase-synchronizing target, which is

sketched as a corner reflector. The corner reflector is shown closer to the radar than the target region. Each antenna element receives an echo trace that contains clutter, the beamforming corner reflector, and the target. The echo waveform from each element is coherently demodulated, sampled in range, and stored in the format shown for image formation. To produce the image the processor must perform several functions: it must find the range element that contains the phase synchronizing source, self-focus a beam on it, refocus the beam to the target range, and scan the beam in azimuth across the target. When these operations are completed, the output of the system is a one-dimensional scan or image of the target. A two-dimensional (range, angle) image is built up from a succession of angle scans.

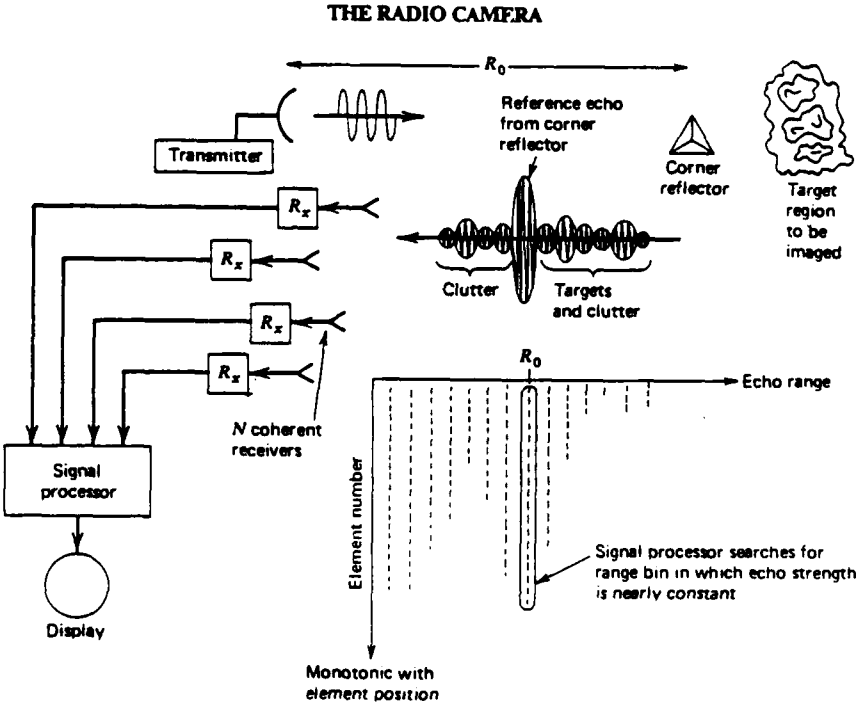

FIGURE 4.1 RADIO CAMERA DATA FORMAT AND PROCEDURES (FROM [2])

The range trace delivered by each antenna element is stored as a row of complex numbers. Successive rows correspond to successive elements in the array. The position of a sample in a row is proportional to range and designates the range bin. The position of a sample in a column designates the array element number and is monotonic with but not necessarily proportional to element position because the array may be distorted.

The first operation of the signal processor after data sampling and storage is a search in range for a good phase synchronizing source; that is, for that echo sequence across the array that most closely approximates the expected field from a point source. That range is designated R_o and is the

range from which the phase synchronizing reference signal is obtained. The radiation field from a point source in free space would be nearly constant in amplitude across the array, whereas the phase differences would disclose the differential distances (modulo wavelength) to the source as well as the differential phase shifts through the receiving elements. A simple test to find the target with a radiation field that most closely approximates that of a point source is to measure the normalized echo amplitude variance at each range. R_o is that range for which the test value is minimum.

Let us denote the echo amplitude from the ith range bin received by the nth element A_{in}. Its mean $\bar{A}_i = (1/N) \sum_{n=1}^{N} A_{in}$ and mean square $\bar{A}_i^2 = (1/N) \sum_{n=1}^{N} A_{in}^2$ are calculated, where N is the number of antenna elements. Its variance is $(1/N) \sum_{n=1}^{N} (A_{in} - \bar{A}_i)^2 = \bar{A}_i^2 - \bar{A}_i^2$. The variance is normalized to $\bar{A}_i^2$ to remove the effect of target strength and range from the calculations. The normalized variance then becomes $\sigma_i^2 = 1 - \bar{A}_i^2 / \bar{A}_i^2$. The rule for finding R_o, then, is to calculate σ_i for all range cells and search for the smallest value. The signal sequence from that range bin becomes the reference signal. Appendix A gives a detailed description of the adaptive beamforming and scanning operations that result in the high resolution microwave image.

It is worthwhile to list the following general features of the algorithm:

1. Simple and fast.
2. Beamforming angle can be anywhere in the illuminated sector (especially for an airborne application where we entirely depend on finding TOO's).
3. Requires individual amplitudes from every element to be communicated to a central processor.

As will be presented later, newly developed techniques allow better performance, reliability and applicablity. The Robust Minimum Variance algorithm enhances the quality of the formed beam and reduces the uncertainty in the beamforming angle significantly. The Spatial Correlation algorithm not only results in a known beamforming angle but also requires local processing only, in the sense that each element needs to communicate only with its first neighbors, which makes it attractive to a cost effective space based radar application.

4.1.2 BEAMFORMER QUALITY

The loss in mainlobe gain, in dB, due to all the random phase errors across a linear array (having a large number of elements) is shown in [1], [2] to be

$$\Delta G \approx 4.3 \sigma_\phi^2 \qquad (4.1)$$

where σ_ϕ^2 is the variance of the phase errors (assumed to be normally distributed) in square radians. The relationship is plotted in Figure 4.2. The loss is minor (<1 dB) for an RMS phase error of about 1/2 rad. The loss grows rapidly as the phase error grows. A 1 rad RMS phase error results in 4.3 dB loss.

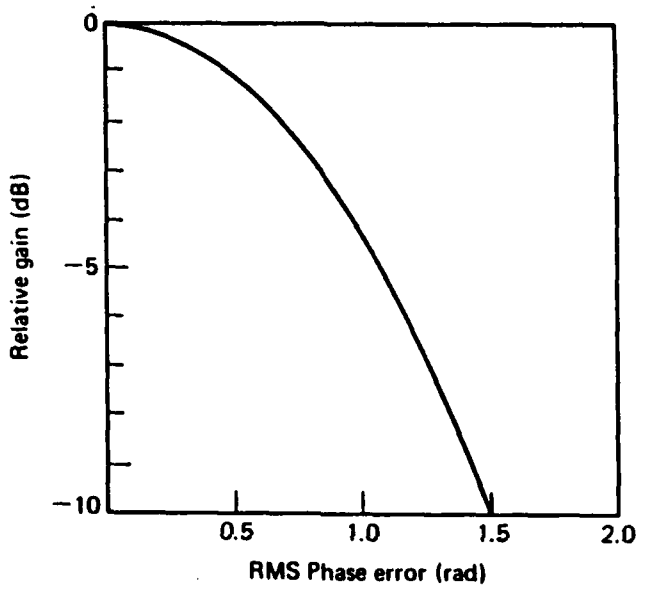

FIGURE 4.2 DECIBEL LOSS IN GAIN DUE TO GAUSSIAN ERRORS (FROM [2])

In our statistical evaluation of the Minimum Variance algorithm the standard deviation $\sigma_{\delta\phi}$ of the residual phase errors across the array at the beamforming angle is used as our measure of quality of candidate beamforming sources. We were able to estimate $\sigma_{\delta\phi}$ because the radar clutter data that we examined were collected by well designed, undistorted arrays with high clutter to noise ratios (the NRL 8-element array and ERIM SAR). This means that the measured phase across the array (for a particular range cell) is almost entirely due to the illuminated clutter patch. In a real-life system of a distributed airborne array, array distortion will obscure the received phasefront and precludes the estimation of $\sigma_{\delta\phi}$.

A good beamformer in the far field of a linear array should produce an almost linear phase across it with the possibility of discontinuities at $\pm\pi$ due to the modulo 2π nature of phase measurements. The slope of the underlying straight line discloses the angular position of the dominant scatterer within the illuminated patch. Retrodirective beamforming forms a beam focused on that scatterer leaving the difference

between the underlying straight line and the measured phase as a residual phase error pattern across the array. To estimate its standard deviation, we first unwrap the phase (if necessary) by adding or subtracting the appropriate multiple of 2π (that removes any discontinuities in the measured phase). A linear regression then follows and the difference $\delta(X)$ between the unwrapped phase and the regression line is obtained. Figure 4.3 illustrates these steps. An estimate of $\sigma_{\delta\phi}$ is obtained as

$$\hat{\sigma}_{\delta\phi} = \left(\frac{1}{N} \sum_{n=1}^{N} \delta^2 \phi_n \right)^{1/2} \qquad (4.2)$$

where N is the total number of antenna array elements. , as given by (4.2), together with (4.1), will be our quality measure.

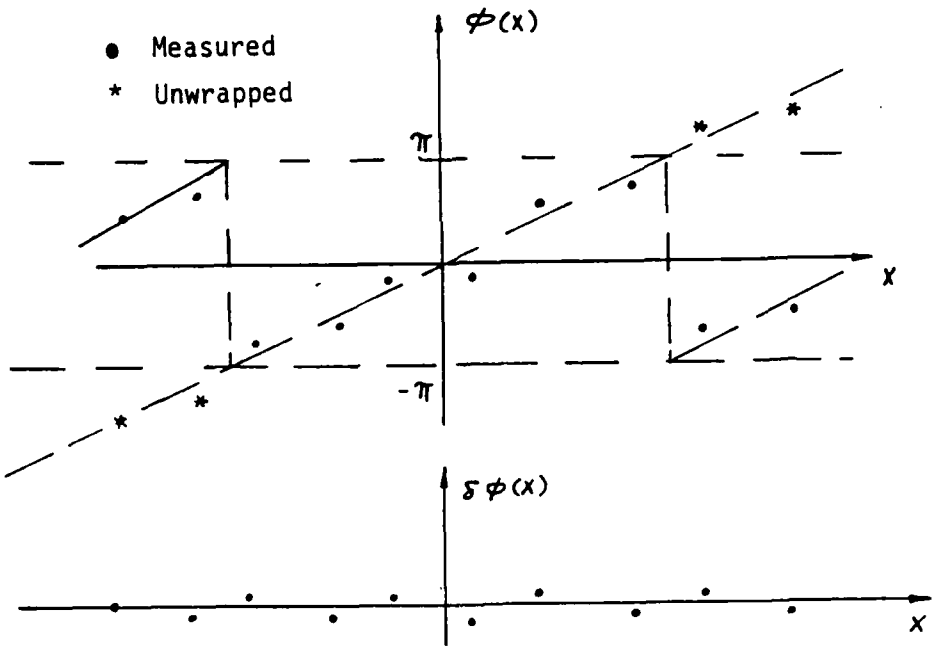

FIGURE 4.3 PHASE UNWRAPPING AND LINEAR REGRESSION

4.1.3 STATISTICS OF $\hat{\sigma}_{\delta\phi}$

In both the NRL 8-element array data and ERIM SAR data we applied the Minimum Variance Algorithm repeatedly on different runs examining each time the range bin that has the minimum amplitude variance and estimated $\sigma_{\delta\phi}$ as described in the previous section. We also examined other range bins that had low amplitude variance. Although we consistently found that the range bin of the minimum amplitude variance had a low $\hat{\sigma}_{\delta\phi}$,

it was not necessarily the best range bin. Other range bins (of low amplitude variance) were often better in the sense that they gave lower $\hat{\sigma}_{\delta\phi}$. We concluded that it is more meaningful to examine the statistics of $\hat{\sigma}_{\delta\phi}$ for these range bins that produced amplitude distributions of low variance. The procedure consists of setting a threshold η_A on the normalized standard deviation of the amplitude, $\hat{\sigma}_{A_i}$, and examining the phases produced by all the range bins that are below this amplitude variation threshold. We then sort the resulting set $\{\hat{\sigma}_{\delta\phi_i} \mid \sigma_{A_i} \leq \eta_A\}$ in an ascending order and produce an estimate of the cumulative distribution function (cdf) of $\hat{\sigma}_{\delta\phi}$.

4.1.4 APPLICATION TO NRL LAND CLUTTER DATA

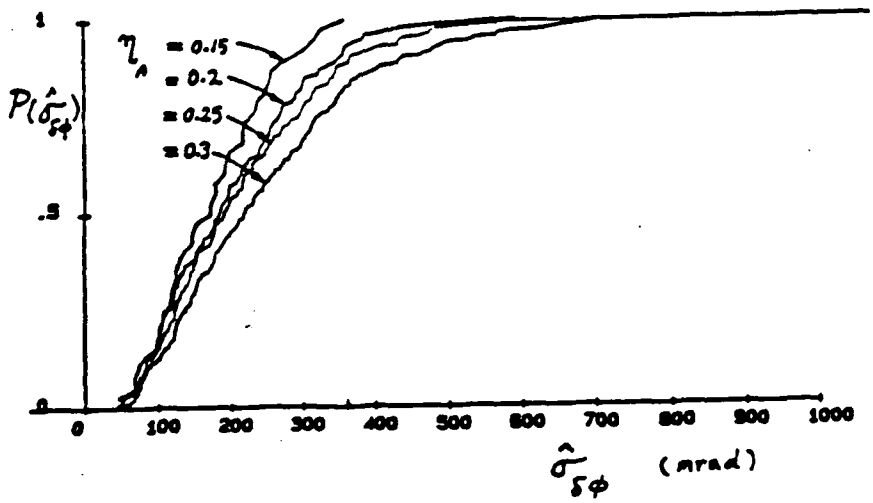

FIGURE 4.4 CUMULATIVE DISTRIBUTION FUNCTION OF THE ESTIMATED STANDARD DEVIATION OF PHASE ERROR (NRL DATA).

Figure 4.4 shows the results of applying the above procedure to some of the NRL 8-element array land clutter runs. The transmit-receive phased array operated at UHF and had $\lambda/2$ spacing between elements. The transmitting pattern was Dolph-Chebyshev weighted for -24 dB sidelobes. The system was flown repeatedly over the south-eastern portion of the United States at about 200 knots at an altitude of 15,000 to 20,000 ft.

Table 4.1 provides important information relating to the family of curves of Figure 4.4. The curves should be used in conjunction with (4.1). For example, a 1 dB loss of mainbeam gain corresponds to $\hat{\sigma}_{\delta\phi} \approx 500$ mrad. For $\eta_A = 0.3$, 95% of the candidate beamformers result in a loss $\Delta G < 1$ dB while for $\eta_A = 0.15$ all the beamformers would result in ΔG equal to or better than 0.6 dB.

TABLE 4.1 PERCENTAGE OF RANGE BINS IN WHICH THE STANDARD DEVIATION OF THE AMPLITUDE DID NOT EXCEED η_A

η_A	.15	.20	.25	.30
N_P	38	101	176	257
N_T	640	640	640	640
Percentage	%5.9	%15.8	%27.5	%40

N = Number of range bins that passed the threshold test
N = Total number of range bins searched

Notice that the results of Figure 4.4 confirm the expected monotonic relationship between amplitude variance and phase variance upon which the Minimum (Amplitude) Variance algorithm is based. This can be seen in the change of slope of $P(\hat{\sigma}_{\epsilon\phi})$ as η_A varies. Mathematically speaking, the relationship is embedded in the Cauchy-Rieman integrals that relate the amplitude and phase of an analytic complex function (such as the electric field received by the array).

Notice also that while a tighter threshold (smaller η_A) results in a set of beamformers of higher quality, the resulting set has less members. The tradeoff between these two factors (quality vs. number) will prove to be important while discussing the newly developed Robust Minimum Variance algorithms later in this report.

4.1.5 APPLICATION TO ERIM SAR LAND CLUTTER DATA

Although the results of the NRL data are highly encouraging (for example, for η_A = 0.15 about 6% of the range bins searched contain satisfactory beamformers (ΔG(0.6 dB)), the results seem to be overoptimistic because the array was used both on transmission and reception. It is simple to show [2] that a transmitting aperture of size D will result in a lobular clutter reradiation patterns of a nominal lobewidth the order of D (in the vicinity of the transmitter). This means that the phase of the received field is expected to slowly vary over a transmit-receive aperture and our chances of finding good beamformers are good to begin with. A more realistic test should involve a bistatic situation where the transmitting aperture is much smaller in size than the receiving aperture. Although we could not find clutter data of exactly this scenario, we realized, however, that we can use SAR data in a way that fits our purposes.

For a relatively short synthetic array of a length much shorter than the cross-range dimension of the illuminated patch, the transmitter moves over a small distance and illuminates almost the same patch of scatterers at each sampling position. The field sampled by the synthetic array will be almost identical to that received by a bistatic system having a receiving array the same size of the synthetic aperture and a transmitter identical to the SAR transmitter.

We obtained several runs of land SAR data from ERIM and formed synthetic arrays of a maximum length of 8 synthetic elements out of a total of 1024 available sampling positions. Figure 4.5 shows the results of a typical run where the SAR operated at X-band with sampling positions taken every 1.5m ($\approx 50\lambda$). The transmitter was about 5 ft in the cross-range dimension and had about -20 dB sidelobes.

In Figure 4.5, we set $\eta_A = 0.2$ and tried different synthetic array lengths ($150\lambda - 400\lambda$, corresponding to 3-8 synthetic elements). As expected, for a given $\hat{\sigma}_{\delta\phi}$ the chance of finding beamformers (of corresponding quality) decreases as the array length increases. This is natural because it takes a small (on a wavelength scale) dominant scatterer to produce a planar phasefront over a large aperture. Such a phase-front will be certainly good for phase-synchronizing a smaller aperture but not necessarily so for a larger one. Table 4.2 gives the percentage of range bins that did not exceed the threshold relative to the total number of range bins examined.

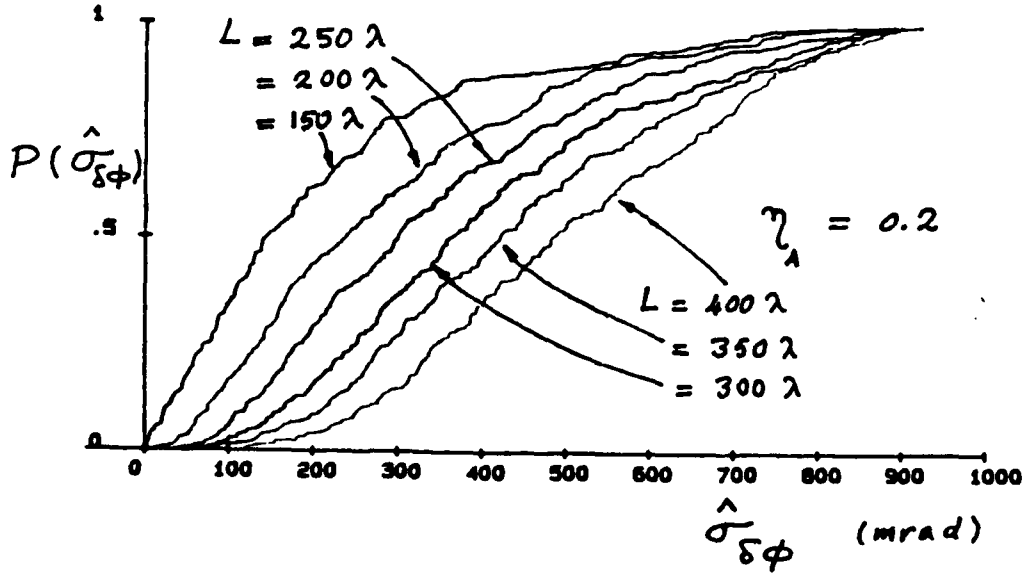

FIGURE 4.5 CUMULATIVE DISTRIBUTION FUNCTION OF THE ESTIMATED STANDARD DEVIATION OF PHASE ERRORS (SAR DATA).

There were 1024 range bins per run. Whenever we needed more range

TABLE 4.2 PERCENTAGE OF RANGE BINS IN WHICH THE STANDARD DEVIATION OF THE AMPLITUDE DID NOT EXCEED $\eta_A = 0.2$

L	150λ	200λ	250λ	300λ	350λ	400λ
N_p	279	277	304	252	238	222
N_T	1,024	2,048	4,096	5,120	9,216	14,336
Percentage	27%	13.5%	7.4%	4.9%	2.6%	1.5%

bins to search (to get a reasonably smooth curve) for a certain array length we formed additional (nonoverlapping) arrays of that particular length. We had no trouble doing so because we have a total of 1024 synthetic array elements available to us.

Figure 4.5 reveals the limitations of the Minimum Variance Algorithm. The algorithm becomes less and less reliable as the array length increases. For example, the curve for L = 400 λ (≈ 12m, about the size of a fighter aircraft) shows that if we pick a single range bin in which the amplitude variation did not exceed $\eta_A = 0.2$ (Table 4.2 shows that only about 1.5% of the available range bins will satisfy this threshold), the chance is about fifty-fifty that it will be useless. The Minimum Variance Algorithm uses a single range bin (the one that has the minimum amplitude variance across the array) as the reference signal. Experiments showed that this range bin is not necessarily the best, and for larger arrays it might not be even good enough. As we will show later (Under Task 4.4), we developed the Robust Minimum Variance Algorithm to provide high quality, reliable beamforming based on a collection of inferior beamformers. For L = 400λ (Figure 4.5), we were able to reduce $\hat{\sigma}_{s\phi}$ to a typical value of about 20 mrad. The algorithm has also the further advantage of allowing for subarray processing that can be used for self-cohering a very large array.

4.1.6 APPLICATION TO SEA CLUTTER

We applied the Minimum Variance Algorithm to the NRL airborne 8-element sea clutter data. We found it highly unreliable. This was expected because of the obvious low chance of finding a dominant scatterer in a sea clutter patch. We tried it anyway because of the simplicity of the algorithm and because

we have the data and the mechanism. It served, however, as a check for the principle and as a justification for going to more sophisticated algorithms for self-cohering on sea clutter.

4.2 Task 2: CLUTTER DATA SOURCES

We obtained airborne clutter data from two sources: the Naval Research Laboratory (NRL) and the Environmental Research Institute of Michigan (ERIM). We are quite satisfied with the amount, quality, and diversity of the data that we acquired. In the following we give a brief description of the data under our disposal.

4.2.1 NRL 8-Element Array Data

The Naval Research Laboratory built an experimental airborne phased array radar system that was flown repeatedly over land and water and collected large amounts of land and sea clutter data under various operating conditions. The system consisted of a rigid, filled, periodic, 8-element, UHF ($\lambda \approx 70$ cm) antenna array that was used for both radar transmission and reception. On transmission, a carefully designed Chybyshev beam was launched (-24 dB Sidelobes), while the 8 independent receivers were sampling the echoes simultaneously on reception.

In each receiver, the chirped echoes were compressed and the coherently detected signal from each range cell was sampled (with 10-bit precision) and stored in a complex in-phase and quadrature form. The range cells were 100 ft. apart. The system operated at one out of two sub-KHz pulse repetition rates that allowed a safe margin of oversampling of the Doppler spectrum at different array pointing angles (aircraft speed was held to about 200 knots and the altitude varied from about 15,000 to 20,000 ft). Array steering was mechanical. The number of pulses (range traces) n_p and the number of range cells recorded per pulse n_R was chosen (according to memory limitations) such that $n_p \times n_R \approx 1500$.

Land clutter data runs were taken from flights over the south eastern portion of the United States. We have runs for $(n_p , n_R) = (66, 192)$ and $(n_p , n_R) = (34, 448)$. For most of the runs we obtained, the array was looking along the ground track of the aircraft. We requested special runs for which the array looked at about 45 degrees relative to the ground track to allow for a reasonable spread in the Doppler spectrum to test the Doppler Beam-Sharpening algorithms (Task 3).

Sea clutter data runs were taken from flights over the Atlantic Ocean off the south eastern shore of the United States. The data we processed corresponded to a moderate sea with the aircraft flying at an altitude of approximately 17,000 ft, with the array broadside pointing at the direction of the aircraft nose. For these data we had $(n_p , n_R) = (3, 5440)$.

4.2.2 ERIM SAR Data

As mentioned earlier, the results of applying the minimum variance algorithm to the NRL data were over optimistic because the array was used both on transmission and reception. A more realistic test should involve a bistatic situation where the transmitting aperture is much smaller in size than the receiving aperture. Although we could not find clutter data exactly fitting this scenario, we realized that we can use SAR data in a way that fits our purposes.

For a relatively short synthetic array of a length much shorter than the cross-range dimension of the illuminated patch, the transmitter moves over a small distance and illuminates almost the same patch of scatterers at each sampling position. The field sampled by the synthetic array will be almost indentical to that received by a bistatic system having a receiving array the same size of the synthetic aperture and a transmitter identical to the SAR transmitter.

We obtained several runs of land SAR data from ERIM and formed nonoverlapping synthetic arrays of a maximum length of 8 synthetic elements out of a total of 1024 available sampling positions. The SAR operated at x-band with sampling positions taken every 1.5m (approximately 50λ). The transmitter was about 5 ft in the cross-range dimension and had about - 20 dB sidelobes. The data were intended for producing SAR images (using digital processing) with azimuth resolution of about 1.44m and range resolution of about 1.5m. The data were compressed in range and each range trace consisted of 1024 range cells.

4.3 Task 3: DOPPLER ALGORITHMS

4.3.1 Doppler Beam Sharpening

Figure 4.6 describes an airborne radar moving with speed V and illuminating a clutter patch with beamwidth $\Delta\theta$ at distance R and at an angle θ from the ground track. The receiving array of length L is assumed to be distributed on the airframe. For a transmitter of size D, $\Delta\theta \approx \lambda/D$ and the clutter patch width $W=R\,\Delta\theta \approx \lambda R/D$. The backscatter from the clutter patch will have a lobular pattern of a nominal lobe width (in the vicinity of the aircraft) of $(\lambda/W)R \approx D$. Typically $D \ll L$ and such a received phasefront is useless for self-cohering the array. By virtue of the aircraft motion, however, echoes from scatterers within the ground patch may be distinguished from one another by their Doppler shifts; hence narrowband filtering of the received

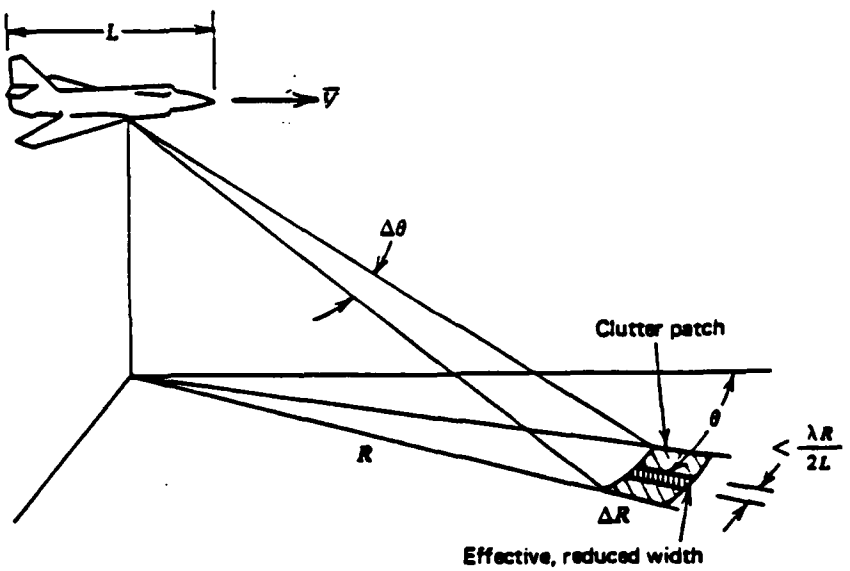

FIGURE 4.6 NARROWBAND FILTERING IN THE RECEIVER REDUCES EFFECTIVE PATCH WIDTH (FROM [2])

clutter echoes can extract the reflections from scatterers within a subpatch of a smaller width. The smaller the subpatch is the wider the lobewidth of the clutter received by the array. To improve the chance of finding a planar (or spherical) phase front suitable for self-cohering the array, the aircraft must be covered by a relatively small portion of a single lobe reradiated from the subpatch. A rule of thumb, derived in [2], requires that the subpatch width to be less than $\lambda R/2L$ (corresponding to a lobewidth of at least twice the size of the aircraft). The Doppler shift of an echo from a scatterer at an angle θ from the ground track is

$$f_d \approx 2v\cos\theta/\lambda \qquad (4.3)$$

Using (4.3), it is shown in [2] that a narrowband filter of bandwidth $B < \frac{v}{L}$ is needed to pass the echoes from the central region of the illuminated ground patch of Figure 4.6, and reject the remainder. This requires an integration time $T \approx B^{-1} > \frac{L}{v}$. The NRL data that we Doppler-processed were collected over a time interval of about $3\frac{L}{v}$, permitting us a good margin for testing Doppler Beam Sharpening. Figure 4.7 shows the results of Doppler-processing an NRL data run. In this run the array broadside made 45 degree angle with the ground track with $(n_x, n_R) = (66, 192)$. The variable parameter here is N_s, the number of pulses (time samples) used in the FFT. For each curve in Figure 4.7 an N_s - point Hamming weighted FFT is computed for every array element for all the range bins. For every range bin, a particular spectral line, corresponding to a certain direction in the clutter

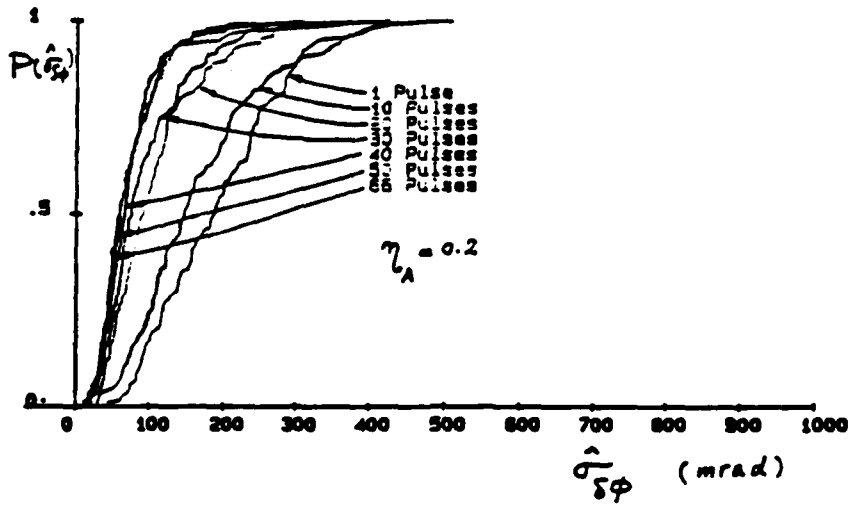

FIGURE 4.7 EFFECT OF DOPPLER BEAM SHARPENING ON THE CUMULATIVE DISTRIBUTION FUNCTION OF THE ESTIMATED STANDARD DEVIATION OF PHASE ERRORS (NRL LAND CLUTTER DATA)

patch, is examined as before. That is, an amplitude variation threshold is set on the normalized RMS of the magnitude pattern of that spectral line across the array; if the range bin passes the threshold, the phase profile is examined, phase unwrapping is made-if needed-followed by linear regression and an estimate of $\hat{\sigma}_{s\phi}$ is obtained. Repeating the procedure for all range bins, a set $\{\hat{\sigma}_{s\phi}\}$ is obtained and sorted to get an estimate of the cumulative distribution function $P(\hat{\sigma}_{s\phi})$. Table 4.3 gives the percentage of range bins that satisified the threshold test relative to the total number of range bins examined.

TABLE 4.3 PERCENTAGE OF RANGE BINS THAT SATISFIED A THRESHOLD TEST AT $\eta_A = 0.2$

N_s	1	10	20	30	40	50	66
N_p	103	109	110	113	240	254	124
N_T	1344	960	768	576	768	768	384
Percentage	%7.7	%11.4	%14.3	%19.6	%31.3	%33.1	%32.3

Notice that N_T is always a multiple of $n_R = 192$. In order to get a reasonably smooth curve of $P(\hat{\sigma}_{s\phi})$, N_p is increased by looking into clutter subpatches of different directions (corresponding to different spectral lines). This was possible for $N_s \geq 20$. For $N_s = 10$, in addition to looking at two different directions, we had to repeat the Doppler processing for few nonoverlapping, well-separated sequences of 10 pulses. For $N_s = 1$, we examined several pulses with as much separation in time as possible.

Notice the dramatic improvement in the statistics of $\hat{\sigma}_{s\phi}$ introduced by Doppler processing. The median decreases significantly as the number of pulses N_s increases. Most of the improvement occurs for $1 \leq N_s \leq 30$. It slows down afterwards. We believe that the slowing is due to a fundamental limit on how narrow a subpatch can be made by Doppler processing. It is implicit in (4.3) that the scatterers are assumed to be completely rigid or "frozen". If the scatterers undergo relative motion with respect to each other due to wind, for example, as in the case of vegetation and sea clutter, the Doppler shift due to a particular scatterer will not only be a function of its angular position but also a function of its own motion relative to the aircraft. In other words, clutter bandwidth puts a limit on the usefulness of Doppler beamsharpening. While it is evident from Figure 4.7 that Doppler beamsharpening is very useful for land clutter, it is shown in [2], [3] that typical clutter bandwidths of sea clutter will render it useless.

Notice also that Figure 4.7 gives a unified approach to the classification of Doppler beamsharpening algorithms. The Minimum Variance algorithm becomes a special case (N_s = 1). As N increases (N_s) 1) we can use a "Hybrid" algorithm where we use all the pulses available to us in a Doppler processing that improves our chances of finding dominant scatterers (by reducing the width of the clutter patch and hence often excluding other scatterers that might be of comparable strength) and then apply the Minimum Variance algorithm to locate (in range) such a dominant scatterer. As N_s becomes large enough to reach the region where the width of the clutter subpatch cannot be made appreciably smaller (limited by the clutter bandwidth) we call it a "Doppler Beamsharpening" algorithm.

4.3.2 Minimum Clutter Bandwidth

As mentioned earlier in the previous section, the above techniques work effectively on narrowband clutter (as found in most land clutter). For relatively wideband clutter, as in the case of heavy vegetation and sea clutter, we have two techniques (see Table 3.1):

-1 Spatial Correlation (non-Doppler)
-2 Minimum Clutter Bandwidth (Doppler)

The second algorithm [3] is quite complex and requires a long convengence time. It uses the spectral bandwidth of the array output as a "quality measure" to determine when the mainbeam is best formed. It was developed before the Spatial Correlation algorithm and mainly served as a proof for the existance of algorithms capable of self-cohering on wind driven land and sea clutter. We listed this algorithm in Table 3.1 for theoretical interest and focused our attention on the Spatial Correlation algorithm instead.

4.4 Task 4: New Algorithm Development

Introduction

We developed several new algorithms during the course of this study. We developed and tested the Robust Minimum Variance algorithm to provide reliable beamforming on a collection of inferior beamformers (targets of opportunity). We also developed and tested the Spatial Correlation algorithm which is applicable to sea as well as to land clutter. It allows also for local processing within the aperture which makes it attractive for a cost effective large aperture space based radar. Finally, we developed a technique of Subarray Processing for applying the above new algorithms to very large airborne/spaceborne radar.

4.4.1 Robust Minimum Variance Algorithm

The minimum variance algorithm uses a single range bin (the one that has the minimum amplitude variance across the array) as the reference signal. Experiments showed that this range bin is not necessarily the best and for larger arrays it might not be even good enough. Also, as a result of beamforming on a single dominant scatterer, the beamforming angle can be anywhere in the illuminated sector. Experiments showed that once an amplitude variation threshold is set, a corresponding number of range bins (on the average) will pass the test. The beamforming quality of these range bins varies, but a considerable number of these will have quality comparable to that of the range bin of minimum amplitude variance. The idea is to use the collection of such candidate beamformers in a phase-smoothing operation that results in a superior "equivalent" phase synchronizing source.

Figure 4.8 illustrates the situation. A quasi-linear receiving antenna array is assumed. The array is distorted both geometrically and electrically. Let us assume that (M+1) range

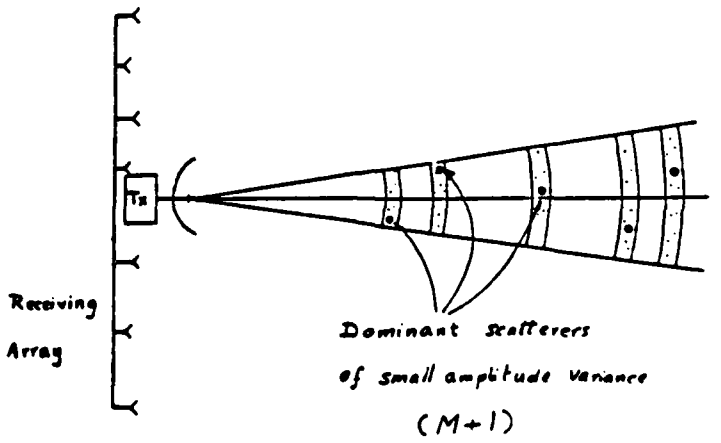

FIGURE 4.8 A QUASI-LINEAR ANTENNA ARRAY IS RECEIVING A Range Trace That Contains M+1 Range Bins With Dominant Scatterers.

range bins passed a low amplitude variation threshold η_A . It is likely that each of them contains a dominant scatterer although the "degree of dominance" might vary from one to another. Assuming far-field conditions, the measured phase by the nth array element due to the ith range bin (that passed the threshold) will have the general form (dropping any constant phase term across the array)

$$\phi_{i,n} = a_i x_n + b_i y_n + \delta\phi_{i,n} + \epsilon_n + 2\pi m_{i,n} \qquad (4.4)$$

where

- a_i : gives the angular position of the ith dominant scatterer
- x_n : the X-position of the nth array element
- b_i : determined by the angular position of the ith source
- y_n : position error of the nth element in the Y- direction
- $\delta\phi_{i,n}$: deviation from planar phase front
- ϵ_n : unknown phase error due to array electrical distortion; assumed to be uniformly distributed between
- $m_{i,n}$: integer to account for the module 2π nature of phase measurements

We would like to average $\phi_{i,n}$ over all possible i. This should reduce the variances of $\delta\phi_{i,n}$, a_i , and b_i . Simple averaging will in general, do more harm than good. Averaging the integer $m_{i,n}$ will produce a random fraction of 2π that would destroy the array coherence. We avoid this problem by substracting first the phase measured at the range bin of minimum amplitude variance, $\phi_{o,n}$, from all others. The difference is

$$\phi_{o,n} - \phi_{i,n} = (a_o - a_i)x_n + (b_o - b_i)y_n + (\delta\phi_{o,n} - \delta\phi_{i,n}) + 2\pi k_{i,n} \qquad (4.5)$$

Notice that ϵ_n is eliminated from (4.5). As a consequence, (4.5) will be almost a straight line in x , with the possibility of a 2π jump whenever the line tries to cross $\pm\pi$. This is illustrated in Figure 4.9. With limited knowledge of element positions, a 2π discontinuity can be easily recognized, allowing

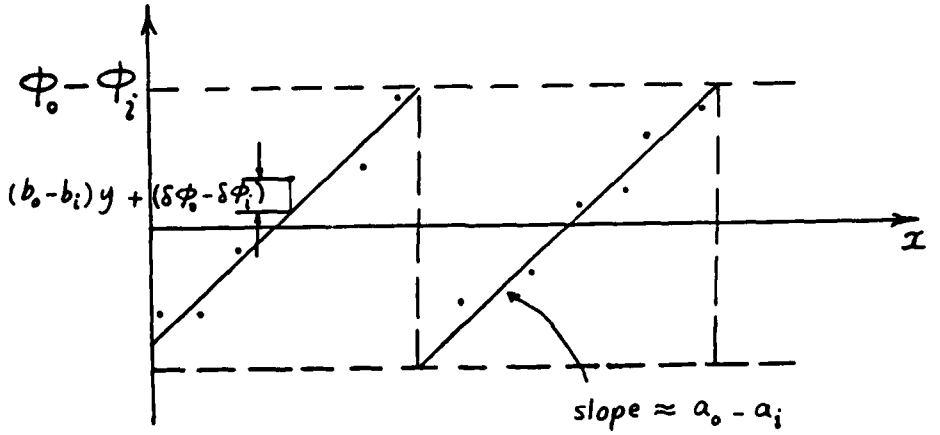

FIGURE 4.9 THE DIFFERENCE CAN BE RECOGNIZED AS A BROKEN STRAIGHT LINE. PHASE UNWRAPPING - IF NEEDED - BECOMES POSSIBLE.

for phase unwrapping by adding or substracting 2π. After checking $(\phi_o - \phi_i)$ for i = 1,..,M and phase unwrapping if necessary, we form the average

$$\psi_n = \frac{1}{M} \sum_{i=1}^{M} (\phi_{o,n} - \phi_{i,n})^u = \phi_{o,n} - \bar{\phi}^u_{i,n} + 2\pi \ell_n$$

where the superscript u stands for "unwrapped" and the bar denotes averaging with respect to i. We get a smoothed "equivalent" beamformer ϕ_n^* by substracting ψ_n from $\phi_{o,n}$

$$\begin{aligned} \phi_n^* &= \phi_{o,n} - \psi_n \\ &= \bar{a}_i x_n + \bar{b}_i y_n + \overline{\delta\phi}_{i,n} + \epsilon_n + 2\pi j_n \end{aligned} \qquad (4.5)$$

Comparing (4.5) and (4.4), we recognize (4.5) as an equivalent phase synchronizing source with the following advantages:

1. $\text{var}\{\overline{\delta\phi_i}\} \cong \frac{1}{M} \text{var}\{\delta\phi_o\}$

2. $\text{var}\{\bar{a}_i\} \cong \frac{1}{M} \text{var}\{a_o\}$

The approximately-equal sign accounts for the fact that dominant scatterers, found in nature, are not necessarily identically distributed in position and phase deviations. The reduced variance of $\overline{\delta\phi_i}$ relates directly to higher beamforming quality, while the reduced variance of $\bar{a}_i$ means a reduced uncertainty in the beamforming angle, i.e., the formed beam will have the extra advantage of being centered in the illuminated sector.

The $\bar{b}_i$ term in (4.5) should be treated carefully. Although geometrical distortion is compensated totally along the beamforming direction in the simple case of retrodirective beamforming (as applied in the minimum variance algorithm), a residual geometrical error in the Y-dimension will be present at the beamforming angle when we use (4.5) for beamforming (element position errors in the X-dimension are compensated totally at the beamforming angle). The reason is that while for a single beamformer $a_i = k\sin\theta_i$, $b_i = k\cos\theta_i$, where k is the wavenumber and θ_i is the angular position of the beamformer relative to array broadside (see Apendix B), we find that for the smoothed beamformer, the beamforming angle $\theta_* = \sin^{-1}\{\bar{a}_i/k\}$ is not necessarily equal to $\cos^{-1}\{\bar{b}_i/k\}$. Fortunately, we will show that the residual geometrical error can be made negligible in most practical cases.

PERFORMANCE

At the beamforming angle, the response to a test target will be characterized by a residual phase error

$$\delta\phi(n) = \delta\phi_1(n) + \delta\phi_2(n) \tag{4.6}$$

where

$$\delta\phi_1(n) = (b_* - \bar{b}_i)\, y_n \ ,$$
$$\delta\phi_2(n) = \overline{\delta\phi}_{i,n} \ ,$$

and $b_* = k\cos\theta_*$. The standard deviation of (4.6) is

$$\sigma_{\delta\phi} = (\sigma^2_{\delta\phi_1} + \sigma^2_{\delta\phi_2})^{1/2} \tag{4.7}$$

In Appendix B, we show that

$$\sigma_{\delta\phi_1} = k\sigma_y \, E^{1/2}\left\{\left([1 - (\overline{\sin\theta_i})^2]^{1/2} - \overline{\cos\theta_i}\right)^2\right\} \tag{4.8}$$

where σ_y , is the standard deviation of y_n .

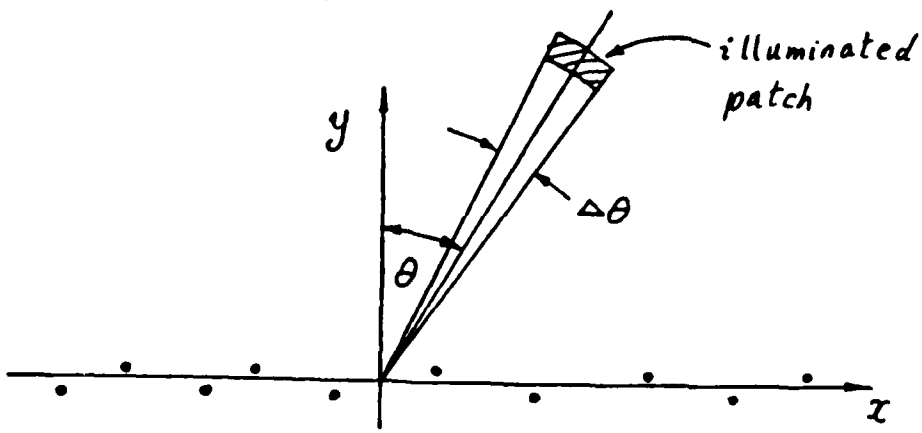

FIGURE 4.10 GEOMETRY USED IN THE COMPUTER SIMULATIONS USED TO ESTIMATE $\sigma_{\delta\phi_1}$.

Although we were able to derive an approximate expression for (4.8), it was quite complex and was not valid for small values of M. We prefered to estimate $\hat{\sigma}_{\delta\phi}$ through computer simulations where we assumed that the angular position of a dominant scatter θ_i is uniformly distributed within an illuminated sector making an angle θ with array broadside and having a width $\Delta\theta$ (Figure 4.10). Appendix B gives the details.

Figure 4.11 plots $\sigma_{\delta\phi}$ as a function of transmitter beamwidth for M=20. Gaussian element position errors in the y-dimension are assumed with standard deviation of 5λ. The transmitter is assumed to make a 10 degree angle with array broadside. In practice, a typical value of $\Delta\theta$ will be about 2 degrees resulting in a negligible geometrical error of less than 2 mrad.

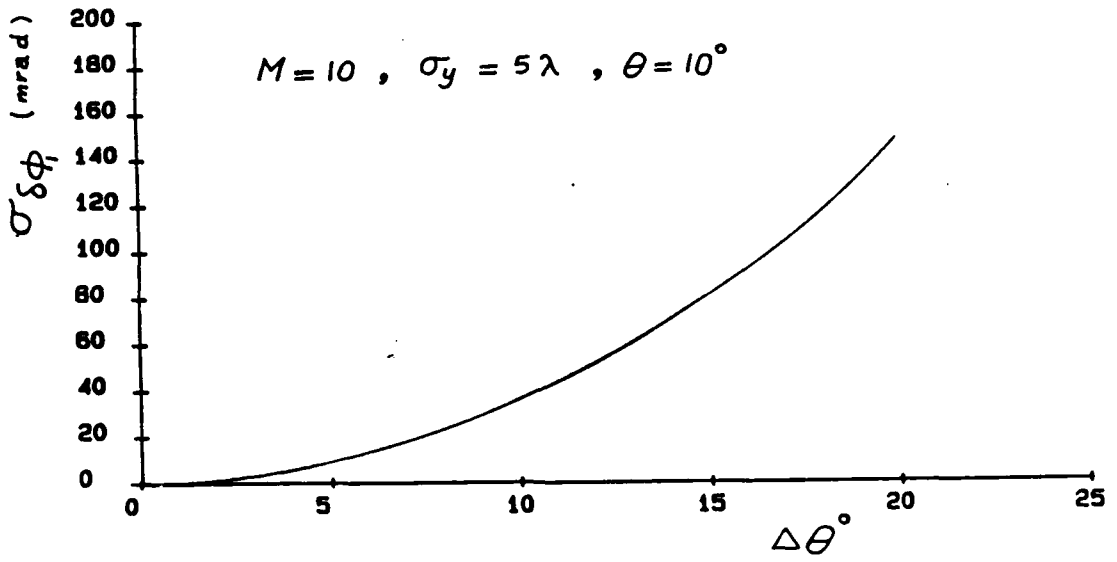

FIGURE 4.11 GEOMETRICAL PHASE ERROR AS A FUNCTION OF TRANSMITTER BEAMWIDTH (COMPUTER SIMULATION).

Figure 4.12 plots $\sigma_{\delta\phi_1}$ as a function of the number of dominant scatterers included in the average, M, for different values of transmitter angle θ. A beamwidth $\Delta\theta$ of 2 degrees is assumed along with Gaussian element position errors of $\sigma_y = 5\lambda$. Notice that the standard deviation of the geometrical phase error vanishes completely for M=1. It rises sharply for $1 < M \lesssim 3$ and becomes almost independent of M afterwards. The sharp increase of $\sigma_{\delta\phi_1}$ as θ approaches 90 degrees is due to the fact that then the array approaches the endfire situation where errors in the y-direction become more important and get magnified. Notice that even in the unlikely scenario of $\theta = 80$ degrees, the standard deviation of geometrical phase errors, $\sigma_{\delta\phi_1}$, is less than 9 mrad and its contribution is quite negligible relative to that of $\sigma_{\delta\phi_2}$ (see (4.7)).

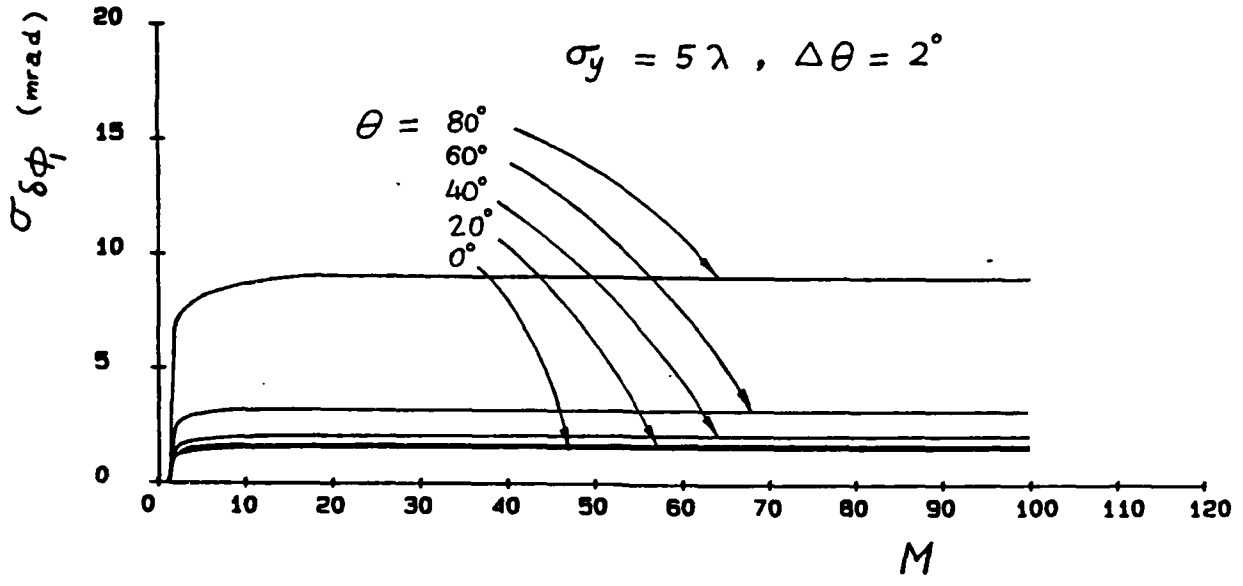

FIGURE 4.12 GEOMETRICAL PHASE ERROR AS A FUNCTION OF THE NUMBER OF DOMINANT SCATTERERS USED IN THE AVERAGE (COMPUTER SIMULATIONS).

Figure 4.13 shows how averaging reduces the variance of the deviation from planar phase front, $\sigma^2_{\delta\phi_1}$, (the part due to mother nature) in a typical application of the robust minimum variance algorithm on ERIM SAR data. The experiment was made with η_A = 0.3 and 1024 range bins were examined. The synthetic array was

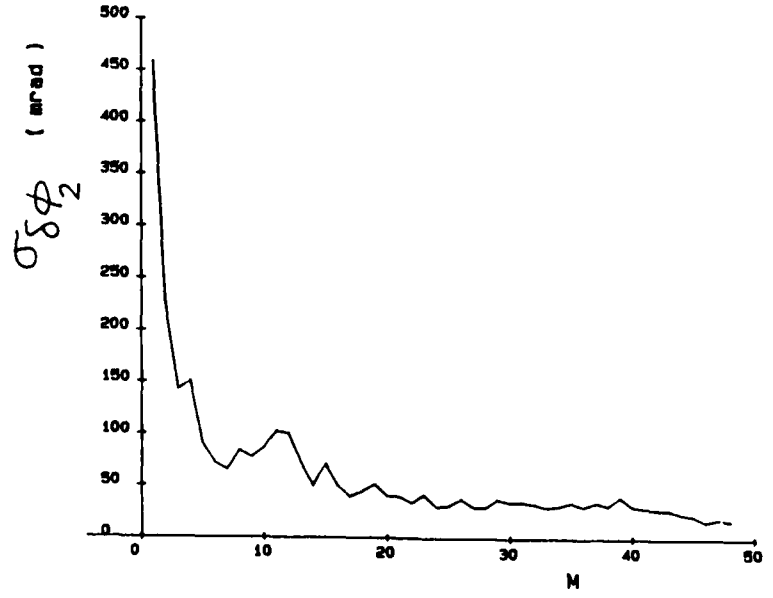

FIGURE 4.13 RESULTS OF APPLYING THE ROBUST MINIMUM VARIANCE ALGORITHM ON A 400λ - SYNTHETIC ARRAY.

400 λ long (see Figure 4.5) and a modified version of the algorithm was used. The improved version of the algorithm selectively includes range bins that already passed the amplitude variation threshold according to whether or not these pass a phase threshold set on the RMS of the regression error. Linear regression is done after phase unwrapping (Figure 4.9). Provided that the dominant scatterer of the lowest amplitude variance has small deviations $\delta\phi_0(n)$ of its own, a larger RMS value of the regression error of $(\phi_0 - \phi_j)$ indicates that the jth range bin should be excluded from the average. A low RMS value of the same quantity indicates either that the jth range bin is good or that $\phi_j(n)$ is very similar to $\phi_0(n)$ for all n which is highly unlikely for an array of large number of elements. For an array of small number of elements, however, one can exclude such coincidences by not relying completely on one range bin for testing all others. More than one range bin can be used to test the rest, and a majority vote or a linear combination rule (of the resulting RMS values) can be used to selectively include or exclude a range bin (that already passed the amplitude variation test) from the average.

Figure 4.13 shows a dramatic reduction in $\hat{\sigma}_{\delta\phi}$. An initial value of about 450 mrad is reduced to about 20 mrad. Assuming a typical residual geometrical error $\sigma_{\delta\phi}$ of 5 mrad, the total residual phase error $\sigma_{\delta\phi} = (\sigma^2_{\delta\phi} + \sigma^2_{\delta\phi})^{1/2} = 20.6$ mrad which, in turn correpsonds to an expected loss in mainbeam gain $\Delta G = 0.002$ dB, which is quite negligible for most practical cases.

In conclusion, the robust *minimum* variance algorithm provides reliable, high quality beamforming using a collection of inferior beamformers. In addition, the formed beam is centered within the illuminated sector. This, by itself, is an important advantage since a beam formed close to an edge of the illuminated sector means a loss of almost half the obtainable field of view. Also since the image is obtained by scanning off the formed beam, azimuth measurements will be relative to the beamforming angle. Since the formed beam is now centered in the illuminated sector, absolute angle measurements will be much more accurate (compared to those obtainable by applying the minimum variance algorithm). Finally, and as we will show later in this section, a centered beam allows for a newly developed technique of subarray processing that can be used to self-cohere a large distributed array.

As a final remark, it is worthwhile to notice that the robust *minimum* variance algorithm uses the range bin of *minimum* amplitude variance in an interesting way. It does not assume that it is the best. It only assumes that it is good enough to enable phase unwrapping of other range bins and actually have a fair look at their phase profiles. The robustness comes from averaging (or selectively averaging) these phase profiles.

4.4.2 SPATIAL CORRELATION ALGORITHM

The spatial correlation algorithm enables self-cohering of distributed arrays in the absences of a beamforming point source, using the spatial correlation properties of radar clutter. It is shown in [4], [5] that if the spatial autocorrelation function of the field (as measured by adjacent element pairs) is ensured to be real and positive in the neighborhood of the origin, both periodic and aperiodic arrays can be synchronized forming retrodirective beams pointing at the axis of symetry of the radar transmitter, provided that the interelement spacing does not exceed some limit (the order of the size of the transmitting aperture).

Figure 4.14 shows a fairly general, quasi-linear (geometrically distorted) antenna array. The array can be both thinned and aperiodic. The elements are connected to a signal processor through cables or any other sort of data link. The quantities through represent a random phase error distribution across the aperture due to uncertainties in cable lengths, impedance mismatches, and perhaps a slowly varying pattern of atmospheric turbulence. In addition, we will lump the differential phase due to the angle of arrival of a plane wave into these quantities. Thus, if we can estimate the δ's we should be able to form a retrodirective beam by substracting them out. In the following, we will show that this is possible.

The ith element delivers a measured field value of $e'_i = e_i e^{j\delta_i}$ where e is the error-free value (excluding the differential phase due to angle of arrival which is included in δ_i) produced by a large number of non-coherent scatterers. The ith correlator provides an estimate $\hat{R}_i$ of the quantity

$$R'_i = E\{ e'_i e'^{*}_{i+1} \} = E\{ e_i e^{*}_{i+1} \} e^{j(\delta_i - \delta_{i+1})}$$
$$= R(d'_i)\, e^{j(\delta_i - \delta_{i+1})}$$

where $d'_i = d_i \cos\theta_0$. The phase of $\hat{R}'_i$, called ψ_i, is the quantity of interest. Assuming that we have good phase estimates $\{ \psi_i \}$, we can approximately write

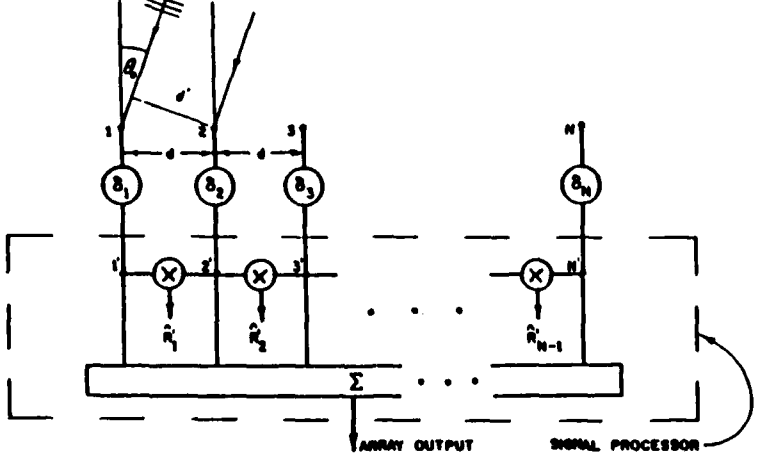

FIGURE 4.14 ARRAY MODEL AND SIGNAL PROCESSOR CONFIGURATION FOR SELF-SYNCHRONIZATION.

$$\psi_i \approx (\delta_i - \delta_{i+1}) + \beta_i \qquad i = 1,2,\ldots,N-1 \tag{4.9}$$

where $\beta_i = \arg\{R(d_i)\}$. Now we form the quantity

$$\phi_i = \sum_{n=1}^{i-1} \psi_n \tag{4.10}$$

$$\approx (\delta_1 - \delta_i) + \sum_{n=1}^{i-1} \beta_n \tag{4.11}$$

which we use as a phase correction by adding it in the ith channel (for all i). The total phase shift becomes

$$\delta\phi_i = \delta_i + \phi_i$$

$$\approx \delta_1 + \sum_{n=1}^{i-1} \beta_n \tag{4.12}$$

Now the phase $\beta(X)$ of the spatial correlation function plays a major role in synchronizing the array. If the spatial correlation function is real and positive in the region of interest ($\beta_i = 0$ for all i) we have an ideal situation, for then (4.12) reduces to

$$\delta\phi_i = \delta_1 = \text{constant independent of } i \tag{4.13}$$

and the random variable δ_i has been replaced by a constant. The result is a well-formed retrodirective beam making an angle θ_0 with array broadside.

It is shown in [4], [5] that R(X) is the Fourier transform of the intensity patterin I(u) associated with the illuminated clutter patch, which by definition is real, it is only necessary to insure that I(u) be symmetric for R(X) to be real. We will show later that this is a practical condition to achieve.

PRACTICAL REALIZATION

The technique described above is based on the assumption of the availability of noncoherent microwave scatterers and on our ability to accurately measure samples of the spatial autocorrelation function of the reradiation from these scatterers. A large number of nonrigid scatterers with random relative motions can provide us with the required noncoherence. Examples are sea waves, moving leaves of a bush or a field of scatterers where the size's are smaller than the resolution cell of the observing instrument. This is a common situation in radar. We can estimate

$R'(X)$ by averaging successive correlation readings (cross products) taken at time intervals larger than the time required to decorrelate the geometry of the individual scatterers. A faster way is to take the cross products from echoes corresponding to successive range cells, provided that the geometrical features of the scatterers are statistically homogeneous over the area of interest. Sea clutter is a good example. Even a rigid but rough terrain can be useful if echoes from successive range cells are statistically the same, i.e., if they can be considered as sample functions drawn from the same random process.

Figure 4.15 shows a radar transmitter of aperture size D. It illuminates a far-field patch of approximate area $R_0 \Delta R \Delta\theta$, where ΔR is the transmitter range resolution and $\Delta\theta$ is the transmitter beamwidth. For an observer at the transmitter site, the field produced by a scatterer at point 1 is equal to the field produced by the same scatterer moved to point 0 and multiplied by the phase delay factor $e^{-jk(R_1 - R_0)}$. Because the phase relationship between the scatterers at points 1 and 0 is completely random, the phase

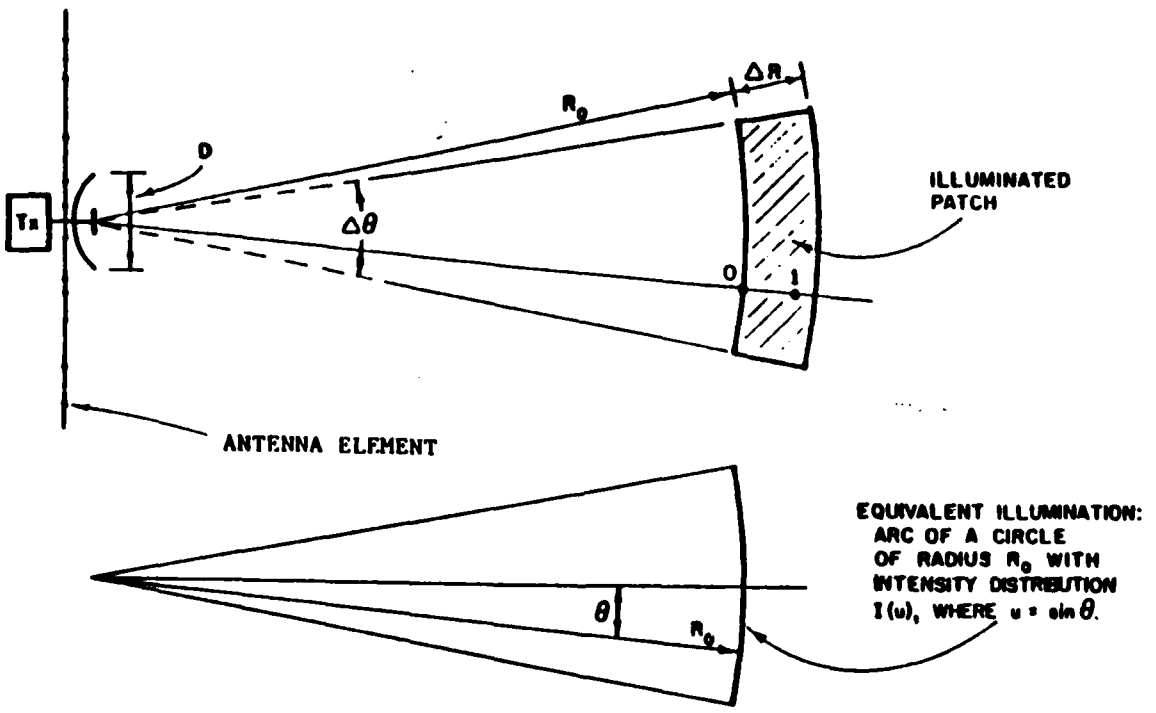

FIGURE 4.15 RADAR ILLUMINATED PATCH AND ITS 1-D EQUIVALENT INTENSITY DISTRIBUTION.

difference between the displaced equivalent of the scatterer at 1 and the actual scatterer at 0 will be random. Thus in principle, all the scatterers along the line 01 can be mapped to the point 0 and the whole illuminated patch can be collapsed into an illuminated arc with illumination intensity I(u). If the illuminated patch contains a large number of statistically homogeneous scatterers, we would expect the intensity I(u) to be proportional to the square of the radiation pattern of the transmitter. Thus if the illumination of the transmitter is symmetrical so too will be I(u), and R(X) will be real. For example, the radiation pattern of a uniformly illuminated aperture will be proportional to $\mathrm{sinc}Du/\lambda$ and I(u) will be proportional to $\mathrm{sinc}^2 Du/\lambda$. The autocorrelation function R(X), being the Fourier transform of I(u), will be triangular with base 2D. In general, the correlation distance will be the order of D. Thus the largest interelement distance in the receiving array should not exceed D (with some margin). Notice that the plane wave model of Figure 4.14 will be a good approximation for most practical situations where, typically, the transmitter pattern has a sufficiently narrow beam (few degrees) and a low sidelobe level.

In summary, the only requirement for R(X) to be ideal is that it be real, which, in turn requires that the scatterers be uniformly distributed within the clutter patch and that the transmitter beam be symmetric (which is typical). A real taper for the transmitting aperture provides the desired symmetry, furthermore, from the symmetry of the problem, it is evident that the beam so formed will point in the direction of the axis of symmetry of the transmitting antenna.

EXPERIMENTS WITH AIRBORNE SEA CLUTTER RADAR DATA

We applied our algorithm to the experimental sea clutter data supplied by the Naval Research Laboratory (NRL). The 8-element system was flown over the Atlantic Ocean repeatedly and collected huge amounts of sea clutter data at a variety of operating conditions. The data we used corresponded to a moderate sea with the aircraft flying at an altitude of approximately 17,000 ft. with the array broadside pointing in the direction of the aircraft ground track.

Because the array was rigid, its proper performance could be predicted and, hence, compared to the performance of our adaptive method. Random, unknown phase errors uniformly distributed over $[-\pi, \pi]$ were inserted in each receiving channel. Figure 4.16 shows the results of applying the algorithm to one such experiment. This excellent agreement is typical of many similar tests.

When clutter patches have the same statistics, echoes originating from neighboring range cells can be treated as sample functions drawn from the same random process. In this situation samples of the spatial correlation function R(X) may be estimated by averaging a large number of correlation readings (cross products), each taken from a different range cell. Thus, echoes due to a single transmitted pulse were used to phase synchronize the entire

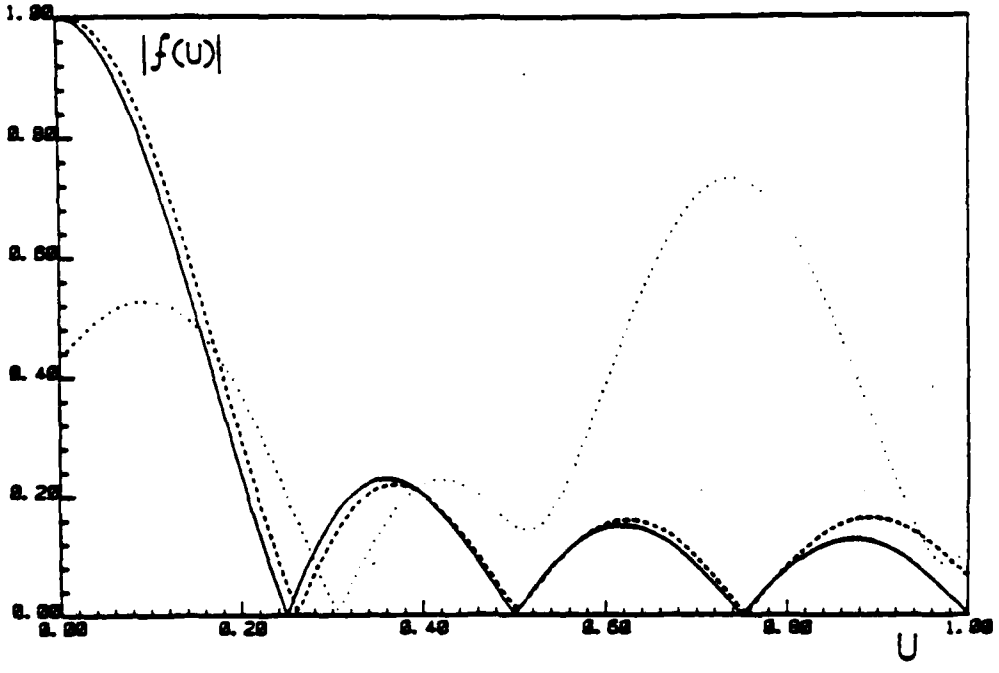

FIGURE 4.16 THE RADIATION PATTERN OF THE 8-ELEMENT PERIODIC ARRAY (FROM [5]).
( ) IDEAL. (...) DISTORTED DUE TO PHASE ERRORS.
(----) RECOVERED BY THE SPATIAL CORRELATION ALGORITHM OPERATING UPON SEA CLUTTER.

array. We used 100 successive range cells starting at 6.4 miles and ending at 8.3 miles. The clutter to noise ratio was about 30 dB. The phase of the estimated autocorrelation values had an estimated standard deviation $\hat{\sigma}_\epsilon$ of 0.097 rad which corresponds to an expected mainbeam gain loss of 0.089 dB (from (3.43), [5]) which is excellent for most applications.

A small beampointing error appears in some experiments; it seems to be zero-mean and its variance is believed to decrease as the number of antenna elements increases. A zero-mean beampointing error indicates a real R(X). This agrees with what we expect since the transmitting beam is symmetric and the roughness of the ocean is fairly homogenous [6].

CONCLUDING REMARKS

In conclusion, we think that it is worthwhile to emphasize the following important features of the spatial correlation algorithm.

1. Simple and fast: it requires a single transmitted pulse for calculating the phase error corrections necessary for real time self-cohering of airborne distributed arrays.

2. Known beamforming angle (if the clutter is homogeneous as in the case of sea clutter): this allows for the application of a newly developed subarray processing technique (described in the next section) that can be used to phase synchronize a very large array.

3. Suitable for sea clutter (as well as land clutter).

4. Allows for local processing: it is straight forward to see from (4.10) that $\phi_{i+1} = \phi_i + \psi_i$, which means that the correction needed for the next element is equal to that needed for the current one plus the angle measured by the correlator connecting them. This means that each element need only to communicate with its first neighbors (as opposed to the case of the minimum variance algorithm where the amplitude received by each element should be sent to a central processor to test for the range bin of minimum amplitude variance). This property makes the algorithm particularly attractive for a cost effective space based radar.

4.4.3 SUBARRAY PROCESSING

It is evident from previous sections that the larger the array size the more difficult self-cohering becomes. Figure 4.5 illustrates the point for the minimum variance algorithm. The robust minimum variance algorithm, however, tolerates larger arrays as long as the phase profile of the range bin of minimum amplitude variance is good enough to permit phase unwrapping of other range bins that passed the amplitude variation threshold and as long as the number of these range bins is large enough to effectively smooth the phase across the compensated array. It is clear that, for a given performance specification (and other design parameters), one can not go beyond a certain maximum array size.

The same is true for the spatial correlation algorithm. As we showed in the previous section, the correction needed for the next array element is equal to that needed for the current one plus the angle measured by the correlator correcting them. Thus errors made in previous correlation measurements (in angle) will propagate across the array putting an upper limit on array size (for a given performance and other design parameters). The effect of error propagation is analyzed in [5].

It is logical to think of dividing a large array into smaller subarrays each of which can be satisfactorily self-cohered using a particular algorithm and then correcting the compensated subarrays somehow in order to straighten out the entire array. The phase profile across a compensated subarray will be approximately a horizontal line with an unknown height that differs from subarray to another as illustrated in Figure 4.17.

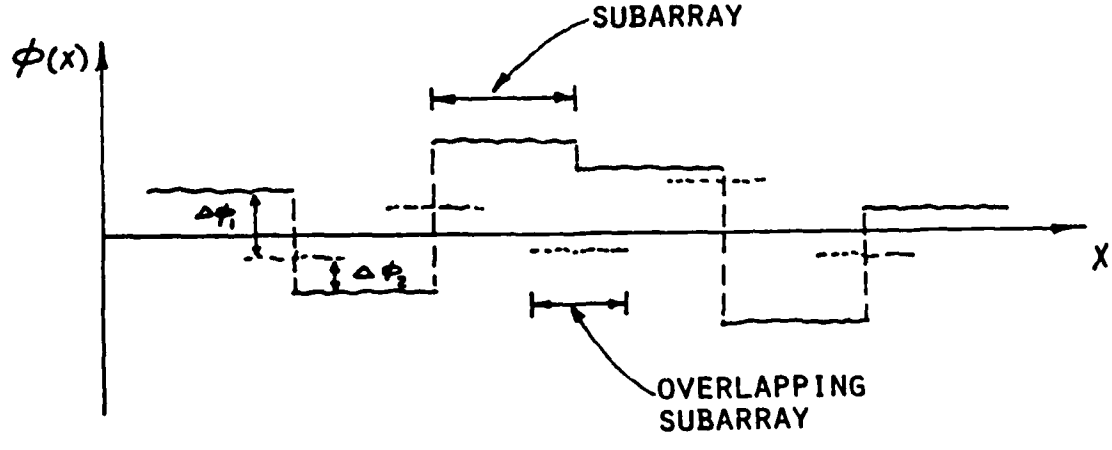

FIGURE 4.17 SUBARRAY PROCESSING

The subarrays cannot be used to form a "superarray" unless phase jumps between adjacent subarrays can be estimated and corrected for. We do not have access to the compensated phase profiles; we only have access to the corrections that our self-cohering algorithms produced. If the subarrays are made to overlap over a number of elements, two sets of corrections will be calculated for each group of elements shared by two subarray neighbors. For each such element, the difference between the two corrections provides an estimate of the phase jump between the two compensated subarrays. Naturally, an estimate based on all the shared elements will be of higher quality. The only problem with making the subarrays overlap is that we are making them longer than necessary this way (and hence making the effort to phase synchronize each of them properly more difficult). A better approach is to let the subarrays be nonoverlapping and form another set of "overlapping" subarrays as illustrated in Figure 4.17. The phase jump between two adjacent subarrays can be estimated on two steps: $\Delta\Phi_1 + \Delta\Phi_2$ (Figure 4.17) with the help of an overlapping subarray.

Notice that an implied condition for the success of the technique is that beams formed by the subarrays should be pointing basically in the same direction. This condition is necessary for forming a high quality "superbeam" based on the entire array. This almost excludes the minimum variance algorithm as a possible vehicle for self-cohering the individual subarrays because then the subarrays are not necessarily focused on the same dominant scatterer and the formed beams will be looking almost anywhere in the illuminated sector. On the contrary, the robust minimum variance and the spatial correlation algorithms fit the procedure naturally since all the formed beams will then be centered in the illuminated sector.

5. CONCLUSIONS

Airborne distributed arrays can be reliably self-cohered on either land clutter or sea clutter. On land clutter, several algorithms exist. Their performances can be improved by Doppler processing and/or robust processing. On sea clutter, the spatial correlation algorithm is the only practical technique and it fits the problem nicely.

Subarray processing is necessary for very large arrays. It employs either the robust minimum variance or spatial correlation algorithm. It makes robust processing applicable to very large arrays and limits error propagation inherent in spatial correlation processing.

Finally, local processing, achieved by the spatial correlation algorithm, can be used with subarray processing for a cost effective implementation of space based radar where the bulk of the processing is done locally, at the element level, using only data from adjacent elements. This obviates the need for transferring large amounts of information to and storing it in a central processing node.

6. RECOMMENDATIONS FOR FUTURE WORK

Work should be continued in the two areas of spatial correlation processing and robust minimum variance algorithms emphasizing subarray processing (as a means of self-cohering very large distributed arrays) and space based SDI applications. For both techniques, consideration should be given to (1) an initial mode in which a subarray is used to illuminate a larger angular sector and the full array is used as multiple beam receiver and (2) iterative self-cohering of the full array for transmit/receive.

6.1 SPATIAL CORRELATION PROCESSING STUDIES

The work should include, but not be limited to, the following:

6.1.1 Develop a two-dimensional spatial-correlation algorithm utilizing subarray processing. This involves the extension of the one-dimensional algorithm to a two-dimensional array of elements in order to take advantage of the fact that the required phase corrections can be estimated more accurately when correlations between an element and all of its 2-D neighbors are utilized.

6.1.2 Perform analysis and computer simulations for optimizing system performance in terms of size and configurations of local clusters of elements and subarrays, pulse width, number of samples, etc.

6.1.3 Evaluate the mainbeam gain and array sidelobe performance in a noise and jamming environment.

6.1.4 Establish candidate 2-D self-cohering systems for use with active sources such as a jammer.

6.2 ROBUST MINIMUM VARIANCE STUDIES

6.2.1 Conduct optimization studies involving subarray processing of large arrays with the robust minimum variance algorithm being used for self-cohering the individual subarrays. This should include investigations about the optimum array size, optimum amplitude variation threshold, and an optimal theory for estimating the phase jumps between subarrays.

6.2.2 Develop a two-dimensional robust minimum variance algorithm. Phase unwrapping should be performed over tilted planes (instead of the 1-D straight lines) in this case. Efficient 2-D phase unwrapping algorithms should be investigated (developed if necessary).

6.2.3 Design and/or simulate an experiment applying the robust minimum variance algorithm in a simulated SDI threat cloud environment where a space-based large antenna array iteratively forms a transmit/receive narrowbeam on a dense pack of flying space object, then scans the beam within the pack in order to image the threat for subsequent identification and classification.

7. REFERENCES

[1] B.D. Steinberg, "Radar Imaging from a Distorted Array: The Radio Camera Algorithm and Experiments," IEEE Trans. Antennas Propag., pp. 740-748, Sept. 1981.

[2] B.D. Steinberg, Microwave Imaging With Large Antenna Arrays, Wiley, New York, 1983.

[3] E. Yadin-Jadlovker, Phase Synchronizing Distributed, Adaptive Airborne Antenna Arrays, Ph.D. Thesis, Univ. of Pennsylvania, Philadelphia, 1981.

[4] E.H. Attia, "Phase Synchronizing Large Antenna Arrays Using the Spatial Correlation Properties of Radar Clutter," National Radio Science Meeting (URSI), Boulder, Colorado, January 1984, Meeting Digest p. 105.

[5] E.H. Attia, Phase Synchronizing Large Antenna Arrays Using the Spatial Correlation Properties of Radar Clutter, Ph.D. Thesis, University of Pennsylvania, Philadelphia, 1984.

[6] M.W. Long, Radar Reflectivity of Land and Sea, Artech House, Dedham, Massachusetts, 1983.

APPENDIX A. THE RADIO CAMERA ALGORITHM

A.1 ADAPTIVE BEAMFORMING

Table A.1 shows all the steps in the procedure. Step 1 initiates the process: $A_{in} \exp(j \psi_{in})$ is the complex envelope of the echo from the ith range bin received by the nth element. Step 2 is the search for R_o. Step 3 is the adaptive beamforming step. The measured phases ψ_{in} can be broken into the sum of two terms $\psi'_{in} + \psi''_{in}$. The first term contains the conventional target and array geometry and is all that would be expected in the absence of array distortion, medium turbulence, multipath, and scattering. The second term represents the errors that the phase

TABLE A.1 STEPS IN RADIO CAMERA IMAGING [1]

Step		
1	Measure and store complex envelopes of echo samples	$A_{in} e^{j\psi_{in}}$ (range bin, element number)
2	Find R_o such that $A_{on} \approx A$, all n	$A e^{j\psi_{on}}$
3	Phase rotate at R_o by phase conjugate in relation to reference element, exp $j(\psi_{oo} - \psi_{on})$	$A e^{j\psi_{oo}}$
4	Phase rotate at all range elements	$A_{in} e^{j(\psi_{in} - \psi_{on} + \psi_{oo})}$
5	focus at each range R_i	$A_{in} e^{j[\psi_{in} - \psi_{on} + \psi_{oo} + (k x_n^2/2)(1/R_i - 1/R_o)]} \triangleq B_{in}$
6	Phase shift linearly with angle	$B_{in} e^{-jk x_n u}$
7	Sum at each range element	$\hat{S}_i(u) = \sum_{n=1}^{N} B_{in} e^{-jk x_n u}$

synchronization process must overcome. In the absence of error the image of the target or clutter from the ith range element would be obtained from the integral of the phase-weighted signals received across the array from the ith range bin. As in any phased array, the phase weighting is the conjugate of the kernel of the diffraction integral. For ease of discussion the diffraction integral can be approximated by the Fresnel integral, which reduces to the Fourier integral when the target is in the far field. The Fresnel integral, in turn, is best represented by a sum, as in (A.1), because the array is discrete. The sum

$$\hat{S}_i(u) = \sum_{n=1}^{N} A_{in} e^{j\psi'_{in}} e^{-jk(x_n u - x_n^2/2R_i)} \qquad (A.1)$$

is the image $\hat{s}_i$ of the scattering sources in the ith range bin, provided that $\psi'' = 0$. We have $u = \sin\theta$ and θ = scan angle from the normal to the array. The discrete variables x_n and R_i are, respectively, the x-coordinate in the array (transverse to the array normal) of the nth element and the distance to the ith range bin.

The function of the adaptive processor is to compensate for ψ''_{in} to allow the operation described by (A.1) to be completed. In the earlier steps of the process the data were searched to find the range bin in which the echo amplitude across the array had the smallest variation. That range bin became the reference range and its signal became the synchronizing signal. Its complex envelope is $A_{on} \exp(j \psi_{on})$, where the amplitudes are all nearly the same. The phases of the echoes, however, are random because of the perturbed geometry of the array, the spatial variations of the refractive index, the impedance variations from element to element, or any combination of these factors. If the reference source were ideal, the phase differences would be due entirely to them. In addition, the phases are perturbed by multipath and scattering. But because it is generally impossible for the system designer to obtain a priori information about these conditions the signal processor must necessarily ignore them.

The third step in the process is to compensate for the phase variations, which are assumed to be due to the first set of factors (i.e., geometry, refractive index, and impedance). Correction is made by phase-rotating the complex envelopes of the signals from R_o received by the different array elements to cophase them. Let some element in the array be designated the reference element and the phase of its signal from the reference range be designated ψ_{oo}. The proper phase shift for the nth element is the negative of the phase difference $\Delta\psi_{on} = \psi_{on} - \psi_{oo}$. The complex signal envelope at the nth element becomes $A_{on} \exp (j \psi_{on}) \exp[- j (\psi_{on} - \psi_{oo})] \approx A \exp(j \psi_{oo})$. This correction, or phase conjugation, is exactly what a phased array or lens would do when focusing on the reference source. The output signal from the array when it is focused is the sum of these phase-corrected echoes from R_o.

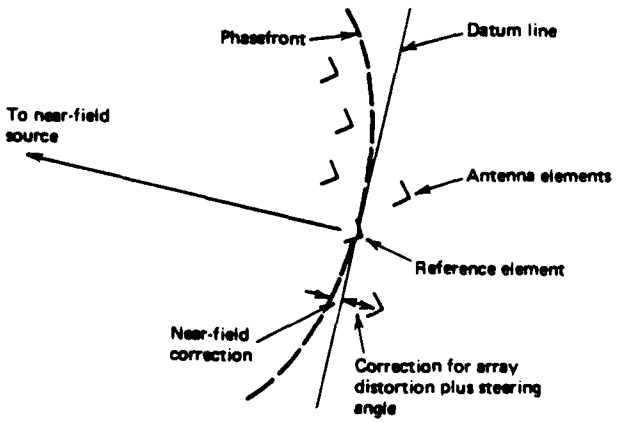

FIGURE A.1 COMPONENTS OF THE PHASE SHIFT IN ADAPTIVE BEAMFORMING.

$\Delta\psi_{on}$, or the differential distance $\Delta\psi_{on}/k$ that it represents, is the sum of two quantities. The first is due to the geometric distortion and includes the steering direction to the source. It is the distance of each element from a datum line or plane in the array that contains the reference element and that is oriented normal to the direction to the synchronizing source, which is the desired correction. When the source is in the near field of the array $\Delta\psi_{on}/k$ also has a second component. It is the added differential distance $x_n^2/2R$ between the spherical phasefront and the datum line. These components of $\Delta\psi_{on}/k$ are illustrated in Figure A.1.

A.2 SCANNING

The fourth step (performed simultaneously with Step 3) is to phase-rotate all the signal samples from each antenna element by $\psi_{on} - \psi_{oo}$. The samples of the complex envelope from the ith range bin now become $A_{in}\exp[j(\psi_{in} - \psi_{on} + \psi_{oo})]$. The sum of a set of complex samples represents the output of a misfocused phased array or lens because $\psi_{in} \neq \psi_{on}$, except at the range R_o of the reference reflector.

The fifth step is to focus the array at all ranges simultaneously. This task is accomplished for an arbitrary range R_i by refocusing the array from the reference range R_o to R_i. The phase correction is approximately quadratic, given by (A.1). Assuming that the earlier steps were performed properly, the self-cohering process forced the quadratic component of the phase shift of the signal in the nth channel to become $-kx_n^2/2R_i + k\,x_n^2/2R_o$. To focus the array to range R_i this term must be set to zero, which requires a further phase addition of $(kx_n^2/2)(1/R_i - 1/R_o)$. This step requires a knowledge of the range R of the reference reflector. Fortunately the value of R_o can be measured (as in conventional radar) by the round-trip travel time of the pulse to the phase synchronizing source and it is read directly into the signal processor from the radar receiver. The accuracy of measurement is determined by the range resolution of the system, which is the order of the reciprocal of the signal bandwidth [in distance units] or the near-field range beamwidth, whichever is smaller.

Step 6 imparts a linear phase rotation to the range-focused complex envelope (designated B_{in} in Table A.1) for each scan angle u. The phase shift is $-kx_n u$.

The last step forms the sum of the linearly phase-weighted, range-focused samples to obtain the image $\hat{s}_i(u)$ for the ith range bin:

$$\hat{s}_i(u) = \sum_{n=1}^{N} B_{in} e^{-jk x_n u} \qquad (A.2)$$

A.3 ELEMENT POSITION TOLERANCE

Steps 2, 3, and 4 require no knowledge whatsoever of element position. The phase synchronization process is purely retrodirective. Steps 5 (refocusing in range) and 6 (scanning in angle) do require coordinate information. The tolerances on element position error have been worked out [1], [2]. The most stringent tolerance is invoked by Step 6. Briefly, the theory consists of the following points:

First, the loss in mainlobe gain, in dB, due to all the random phase errors across the array is shown to be $\Delta G \approx 4.3\ \sigma_\phi^2$, where σ_ϕ^2 is the variance of the phase errors in square radians.

Second, the phase variance due to random position errors is approximately $\sigma_\phi^2 \approx k^2 \sigma_x^2 \theta^2$, where σ_x^2 is the position error variance in the array in the direction perpendicular to the beamforming direction and θ (rad) is the scan angle measured from the direction of beamforming. Combining these expressions and allowing 1-dB loss in array gain as an accepatable gain-loss tolerance, the rms element tolerance becomes $\sigma_x \approx (\lambda/4\pi)\theta_{max}^{-1}$.

The factor $\lambda/4\pi$ is the conventional tolerance in phased array, mirror, or lens design; θ_{max} is the maximum scan angle from the direction of the reference source and is half the field of view. Because an individual radar target always subtends a small angle at the radar, $\theta_{max} \ll 1$ and the allowed element position error is exceedingly large; for example, if the system were designed to image a target as large (in angle) as the moon, θ_{max} would be approximately 10^{-2} rad. In this case the position accuracy tolerance increases by two orders of magnitude to about 10λ. It is precisely the extraordinary liberty in position tolerance, following adaptive phase synchronization, that permits radio camera imaging with a nonrigid or ill-surveyed array.

APPENDIX B. STATISTICS OF GEOMETRICAL PHASE ERRORS

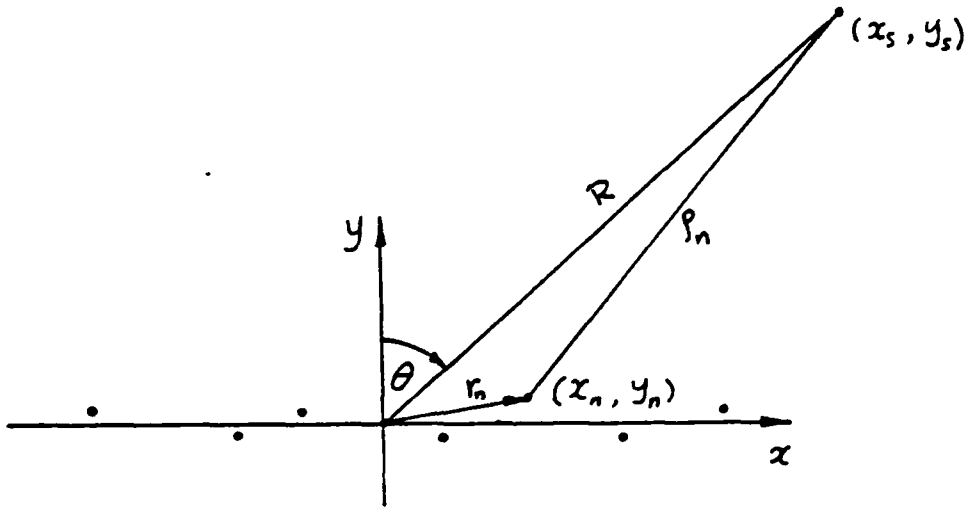

FIGURE B.1 A TWO-DIMENSIONAL GEOMETRY OF A QUASI-LINEAR ARRAY EXCITED BY A POINT SOURCE.

Figure B.1 illustrates a quasi-linear array laid along the x-axis and excited by a point source making an angle θ with array broadside. From the geometry, the distance ρ_n between the source at (x_s , y_s) and the nth array element at (x_n , y_n) is given by

$$\begin{aligned} \rho_n &= [(x_s - x_n)^2 + (y_s - y_n)^2]^{1/2} \\ &= [(R\sin\theta - x_n)^2 + (R\cos\theta - y_n)^2]^{1/2} \\ &= R\left[1 + \frac{r_n^2}{R^2} - \frac{2}{R}(x_n \sin\theta + y_n \cos\theta)\right]^{1/2} \end{aligned} \qquad \text{(B.1)}$$

Expanding (B.1) and retaining the first order terms in the binominal expansion we get the Fresnel (near field) approximation

$$\rho_n \approx R + \frac{r_n^2}{2R} - (x_n \sin\theta + y_n \cos\theta) \qquad \text{(B.2)}$$

If we further assume that $(r_n^2/R) \ll 1$, we get the Fraunhofer (far field) approximation

$$\rho_n \approx R - (x_n \sin\theta + y_n \cos\theta) \qquad \text{(B.3)}$$

and the difference in phase retardation (relative to the origin) sensed by the nth element is

$$-k\Delta\rho_n = k\sin\theta\, x_n + k\cos\theta\, y_n \qquad \text{(B.4)}$$

If we have a number of non-ideal isolated sources (separated in range), the phase measured at the output of the nth receiving channel of the distorted array due to the ith source is

$$\phi_{i,n} = \{ k \sin\theta_i \, x_n + k \cos\theta_i \, y_n + \delta\phi_{i,n} + \epsilon_n \}_{\text{mod } 2\pi}$$

$$= a_i x_n + b_i y_n + \delta\phi_{i,n} + \epsilon_n + 2\pi m_{i,n} \qquad \text{(B.5)}$$

where

$a_i = k \sin\theta_i$,
$b_i = k \cos\theta_i$,
$\delta\phi_{i,n}$ = deviation from planar phase front,
ϵ_n = unknown phase error pattern due to array electrical distortion; assumed to be uniformly distributed between $-\pi$, $+\pi$,
$m_{i,n}$ = integer to account for the modulo 2π nature of phase measurements.

As discussed in section (4.4) if we have (M+1) sources, the one that has the minimum amplitude variance is used to phase unwrap the rest so that their phases can be averaged to produce the equivalent smoothed source

$$\phi_n^* = \bar{a}_i \, x_n + \bar{b}_i \, y_n + \overline{\delta\phi}_{i,n} + \epsilon_n + 2\pi j_n \qquad \text{(4.5)}$$

In the radio camera algorithm (Appendix A), the beamformer phase is substracted from the phases of all range bins and a scanning term is applied to image each range bin in azimuth. To evaluate the quality of (4.5) as a beamformer, we first substract it from the array response to an ideal test target (a point source)

$$\phi_{T,n} = a_T x_n + b_T y_n + \epsilon_n + 2\pi \ell_{T,n} \qquad \text{(B.6)}$$

The difference (modulo 2π) is

$$\phi_{T,n} - \phi_n^* = (a_T - \bar{a}_i) x_n + (b_T - \bar{b}_i) y_n - \overline{\delta\phi}_{i,n} \qquad \text{(B.7)}$$

We then scan the test target in angle. The peak of the magnitude pattern occurs (within a very good approximation) at

$$a_T = a_* \triangleq \bar{a}_i$$

and the residual phase error at the beamforming angle becomes

$$\delta\phi(n) = (b_* - \bar{b}_i)\, y_n - \overline{\delta\phi_{i,n}}$$

$$= \delta\phi_1(n) + \delta\phi_2(n) \qquad \text{(B.8)}$$

where

$$\delta\phi_1(n) = (b_* - \bar{b}_i)\, y_n \ ,$$

$$\delta\phi_2(n) = -\overline{\delta\phi_{i,n}}$$

and

$$b_* = k\cos\left\{\sin^{-1}(\bar{a}_i / k)\right\} .$$

Assuming that the element position error in the y-dimension, y_n, is a zero mean random variable independent of $\bar{b}_i$ and $\overline{\delta\phi_{i,n}}$, it is straighforward to show that the covariance between $\delta\phi_1(n)$ and $\delta\phi_2(n)$ is zero. Thus, the standard deviation of (B.8) is

$$\sigma_{\delta\phi} = \left[\sigma^2_{\delta\phi_1} + \sigma^2_{\delta\phi_2}\right]^{1/2} \qquad \text{(B.9)}$$

In the following, we simulate $\delta\phi_1(n)$ (and hence estimate $\sigma_{\delta\phi_1}$) while we present typical values of $\sigma_{\delta\phi_2}$ in section 4.4 (based on ERIM SAR data).

The variance of $\delta\phi_1(n)$ is calculated as

$$\sigma^2_{\delta\phi_1} = \mathrm{var}\left\{(b_* - \bar{b}_i)\, y_n\right\}$$

$$= E\left\{(b_* - \bar{b}_i)^2\right\} E\left\{y_n^2\right\} - \left(E\left\{b_* - \bar{b}_i\right\}\right)^2 \left(E\left\{y_n\right\}\right)^2 \qquad \text{(B.10)}$$

where we took advantage of the assumed independence of y_n and both b*, $\bar{b}_i$. Furthermore, since y_n is assumed to be zero-mean, (B.10) is simplified to

$$\sigma^2_{\delta\phi_1} = \sigma_y^2\, E\left\{(b_* - \bar{b}_i)^2\right\}$$

$$= k^2 \sigma_y^2\, E\left\{\left(\cos\left[\sin^{-1}(\overline{\sin\theta_i})\right] - \overline{\cos\theta_i}\right)^2\right\} \qquad \text{(B.11)}$$

That is

$$\sigma_{\delta\phi_1} = k\,\sigma_y\, E^{1/2}\left\{f^2(\underline{\theta})\right\} \qquad \text{(B.12)}$$

where

$$f(\underline{\theta}) = (1 - [\overline{\sin\theta_i}]^2)^{1/2} - \overline{\cos\theta_i} \qquad \text{(B.13)}$$

We estimated $E\{f^2(\underline{\theta})\}$ by simulating $f(\underline{\theta})$ on the computer where we assumed that the angular position of a dominant scatterer θ_i is uniformly distributed within an illuminated sector making an angle θ with array broadside and having a width $\Delta\theta$ (Figure 4.10). Equation (B.12) is then used to estimate $\sigma_{\delta\phi_1}$. In all the simulation experiments we performed the sample size was always made large enough to ensure smooth $\sigma_{\delta\phi_1}$ curves.